Petrogenesis of arc lavas from the Rucu Pichincha and Pan de Azucar volcanoes (Ecuadorian arc): Major, trace element, and boron isotope evidences from olivine-hosted melt inclusions

Marion Le Voyer, Estelle F. Rose-Koga, Muriel Laubier, Pierre Schiano

Geochemistry Geophysics Geosystems G3
AN ELECTRONIC JOURNAL OF THE EARTH SCIENCES
Published by AGU and the Geochemical Society

Article
Volume 9, Number 12
30 December 2008
Q12027, doi:10.1029/2008GC002173
ISSN: 1525-2027

Petrogenesis of arc lavas from the Rucu Pichincha and Pan de Azucar volcanoes (Ecuadorian arc): Major, trace element, and boron isotope evidences from olivine-hosted melt inclusions

Marion Le Voyer and Estelle F. Rose-Koga
Laboratoire Magmas et Volcans, OPGC-UBP, IRD, CNRS, 5 rue Kessler, F-63038 Clermont-Ferrand, France (M.Levoyer@opgc.univ-bpclermont.fr)

Muriel Laubier
Laboratoire Magmas et Volcans, OPGC-UBP, IRD, CNRS, 5 rue Kessler, F-63038 Clermont-Ferrand, France

Now at Department of Earth and Planetary Sciences, Harvard University, Cambridge, Massachusetts 02138, USA

Pierre Schiano
Laboratoire Magmas et Volcans, OPGC-UBP, IRD, CNRS, 5 rue Kessler, F-63038 Clermont-Ferrand, France

[1] Primary melt inclusions in olivine phenocrysts (Fo_{74-89}) of basic lavas from Pichincha and Pan de Azucar volcanoes (in the front and rear arcs of the Ecuadorian Andes, respectively) were analyzed by electron microprobe for major elements and by ion microprobe for trace element and boron isotope compositions. Although melt inclusions in the most magnesium-rich olivines contain relatively primitive magmas, their compositions are not directly linked to those of the whole rocks through a differentiation scheme. They are characterized by nepheline-normative compositions with low SiO_2 contents (39.8–47.9 wt%) and unusually high CaO contents (up to 15.4 wt%), which cannot be derived from melting of a simple peridotitic mantle. We explain their formation by the presence of amphibole-bearing olivine-clinopyroxenites in the source of these melts. The trace elements patterns of the melt inclusions show the typical trace element features of arc magmas, such as enrichment in LILE and LREE, and negative anomalies in Nb and Ti. Across-arc variations of mobile versus less mobile incompatible element ratios indicate a decreasing input of a mobile phase from the slab to the mantle wedge with the distance to the trench, along with a decrease in the degree of melting. Boron isotope compositions are highly variable within each volcano ($\delta^{11}B$ from -9.5 ± 1.3‰ to $+3.5 \pm 1.4$‰ for the Pichincha melt inclusions and from -17.9 ± 0.8‰ to -1.9 ± 1.4‰ for the Pan de Azucar melt inclusions) and suggest trapping of isotopically heterogeneous melts. Modeling of both dehydration and fusion of the slab indicates that the Pichincha melt inclusions were formed by melting a source enriched by the addition of 1% of a heterogeneous aqueous fluid derived from the dehydration of both the sediments and the altered oceanic crust (after 74 and 76% of B loss, respectively). The phase that metasomatizes the source of the Pan de Azucar melt inclusions can be either an input of 0.1% of a heterogeneous aqueous fluid or more likely 0.5–1% of a heterogeneous silicate melt.

Components: 14,431 words, 11 figures, 7 tables.

Keywords: melt inclusions; boron isotopes; subduction; Ecuador.

Index Terms: 1043 Geochemistry: Fluid and melt inclusion geochemistry; 1042 Geochemistry: Mineral and crystal chemistry (3620); 1031 Geochemistry: Subduction zone processes (3060, 3613, 8170, 8413).

Received 15 July 2008; **Revised** 1 October 2008; **Accepted** 29 October 2008; **Published** 30 December 2008.

Le Voyer, M., E. F. Rose-Koga, M. Laubier, and P. Schiano (2008), Petrogenesis of arc lavas from the Rucu Pichincha and Pan de Azucar volcanoes (Ecuadorian arc): Major, trace element, and boron isotope evidences from olivine-hosted melt inclusions, *Geochem. Geophys. Geosyst.*, *9*, Q12027, doi:10.1029/2008GC002173.

1. Introduction

[2] Ecuador is located in the northern part of the Andean cordillera, an orogenic belt formed by the eastward subduction of the Nazca plate beneath the South American margin (Figure 1a). During the Plio-Quaternary period, this convergent margin has been responsible for a large magmatic activity, mostly expressed by eruptions of typical calc-alkaline arc lavas. At the latitudes of Ecuador, the Carnegie Ridge (Figure 1a), i.e., the Galapagos hot spot track on the Nazca plate, collides with the South American plate. It was suggested that the shallow dip of the downgoing plate (25–30°) [*Guillier et al.*, 2001] is caused by the subduction of the Carnegie Ridge and controls the surface expression of volcanism. Indeed, chemical characteristics of Ecuadorian lavas indicate that slab melts participate in their formation [e.g., *Monzier et al.*, 1997; *Bourdon et al.*, 2003; *Samaniego et al.*, 2005]. Within the three volcanic alignments that compose the Ecuadorian volcanic arc, only a few volcanoes have erupted basaltic products, and most of them are located in the rear arc [*Bryant et al.*, 2006; *Hoffer*, 2008].

[3] To characterize the compositions of Ecuadorian primary magmas and the nature of their source regions, we have investigated the major and trace element compositions of primary melt inclusions preserved in olivine phenocrysts. The distribution of the melt inclusions in the crystals is not controlled by healed fractures (as might be expected for inclusions of secondary origin). Only primary melt inclusions trapped in polyhedral olivine crystals (grown at slow cooling rate) were chosen because they represent drops of instantaneous melts that have been formed in thermodynamic equilibrium with their hosts [*Faure and Schiano*, 2005]. Their compositions thus record intermediate steps in the evolution of magmas [e.g., *Roedder*, 1984; *Sobolev*, 1996; *Schiano*, 2003]. In the early formed crystals, they could record samples of mantle-derived melts that were trapped prior to fractionation and/or crustal contamination at shallow levels. Therefore, they provide valuable information on the conditions of formation of primitive magmas beneath the Ecuadorian volcanoes.

[4] In order to constrain the nature of the slab input recorded in the chemistry of olivine-hosted primary melt inclusions from Ecuadorian lavas, we performed in situ measurements of boron concentrations and boron isotope compositions. The boron isotopic system is an especially valuable tracer of recycled crustal material from subduction zones [e.g., *Morris et al.*, 1990; *Ishikawa and Nakamura*, 1994; *Palmer and Swihart*, 1996; *Hervig et al.*, 2002] because (1) B is concentrated in the sediments and the altered oceanic crust relative to the mantle wedge, (2) the B isotope compositions of these different reservoirs are contrasted, and (3) B is mobile during both partial melting and dehydration processes.

[5] In this paper, we characterize the compositions of primary olivine-hosted melt inclusions from two volcanoes from the Ecuadorian volcanic arc, Pichincha and Pan de Azucar, by examining a new data set of electron microprobe (major elements) and ion microprobe (trace elements and boron isotope compositions) analyses. Then, we discuss the chemistry of the source of the trapped melts and the slab contribution to the mantle wedge.

2. Geological Setting

[6] Pichincha and Pan de Azucar volcanoes are located in the front arc and rear arc of the Ecuadorian Andes, respectively (Figure 1b). They are 230 and 330 km away from the trench, respectively. They rest on accreted oceanic terranes [*Reynaud et al.*, 1999] and a sedimentary basin above continental bedrock [*Van Thournout et al.*, 1992], respectively. On the basis of whole rock isotopic compositions, crustal contamination plays a minor role in the evolution of Ecuadorian lavas (<10%) [*Bryant et al.*, 2006].

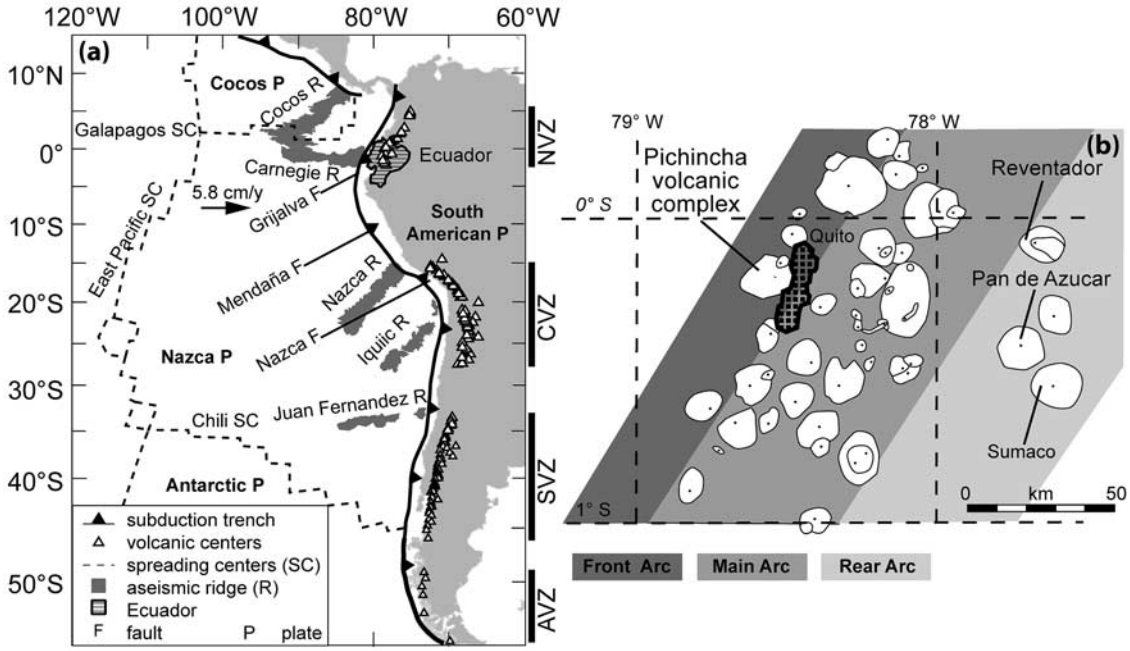

Figure 1. (a) Schematic map of the Andean volcanic and tectonic contexts (modified from [*Gutscher et al.*, 1999]), showing the different volcanic zones of South America and the tectonic features characteristic of the Andean subduction. In front of the Ecuadorian margin, the Carnegie Ridge is subducted beneath the South American plate. The black arrow corresponds to the subduction vector of the Nazca plate relative to South America [*Trenkamp et al.*, 2002]. (b) Location of the Pichincha (in the front arc, dark gray) and Pan de Azucar (in the front arc, light gray) volcanoes within the three volcanic arcs of Ecuadorian volcanoes (white edifices, grouping from *Monzier et al.* [1999]).

[7] Pichincha is a complex stratovolcano. Its activity, expressed mainly by andesitic to dacitic lava and pyroclastic flows (Figure 2a), has been separated into three phases, following the building and collapse of three main edifices: El Cinto (1.1–0.9 Ma), Rucu Pichincha (0.85–0.1 Ma), and Guagua Pichincha (60 Ka, still active and more explosive) [*Monzier et al.*, 2002; *Fornari et al.*, 2004; J.-L. Le Pennec, personal communication, 2008]. The latter is monitored due to the proximity of the city of Quito, 11 km away (Figure 1b). The stratovolcano Pan de Azucar is hardly accessible because of its location in the Amazonian jungle, between Sumaco and Reventador volcanoes (Figure 1b). A full description of Pan de Azucar volcano is found in the work of *Hoffer* [2008]. Presently nonactive, it has been dated to 1.15 ± 0.07 Ma and has produced lavas that can be

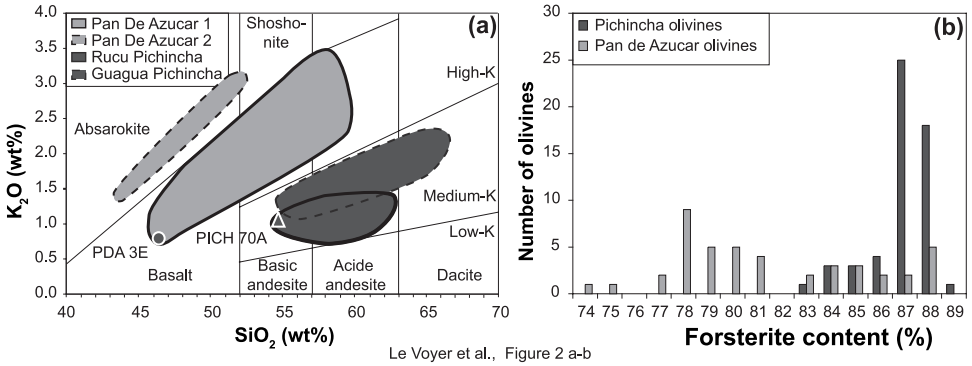

Figure 2. (a) K_2O versus SiO_2 classification diagram of volcanic products from Pichincha volcano (dark gray) [*Bourdon et al.*, 2003] and Pan de Azucar volcano (light gray) [*Hoffer*, 2008]. The two symbols are samples PICH70A and PDA3E containing the melt inclusions of this study. (b) Frequency histogram of the forsterite content of the olivine phenocrysts from Pichincha (dark gray) and Pan de Azucar (light gray) volcanoes.

divided into two high-K series, from basalts to andesites (Figure 2a) [*Hoffer*, 2008].

[8] Their chemical compositions have led several authors to propose that lavas from both Pichincha volcanic complex (named Pichincha hereafter) and Pan de Azucar volcano originate from mantle sources previously metasomatized by slab-derived silicate melts [*Bourdon et al.*, 2003; *Hoffer*, 2008]. In addition, high-magnesium andesites from Pichincha have also been interpreted as slab melts enriched in Mg (and other compatible trace elements) during the ascent through the mantle wedge [*Bourdon et al.*, 2003]. However, others have considered that Pichincha lava compositions are better explained in a more classical way; that is, melting of the mantle wedge enriched by hydrous fluids released from the slab, then crystal fractionation and, to a lesser extent, crustal contamination [*Garrison and Davidson*, 2003; *Bryant et al.*, 2006].

3. Sample Description

[9] Andesites or more evolved lavas form the main types of deposits in Ecuador. As evolved samples are not ideal for the study of primitive melt inclusions, the selected samples in the Pichincha and Pan de Azucar series are the ones with the lowest SiO_2 and the highest MgO contents, therefore considered most primitive. PICH70A (sampled on the Rucu Pichincha edifice [*Monzier et al.*, 2002]) and PDA3E (sampled on the North-West flank of the Pan de Azucar [*Hoffer*, 2008]) are basaltic andesitic and basaltic lava flows, respectively. They have 54.8 wt% SiO_2, 7.6 wt% MgO and 46.6 wt% SiO_2, 10.3 wt% MgO, respectively [*Bourdon et al.*, 2003; *Hoffer*, 2008] (Table 1, Figure 2a). They contain olivine phenocrysts, with forsterite contents ranging from 83 to 89% for PICH70A and from 74 to 88% for PDA3E (Figure 2b).

[10] Primary olivine-hosted melt inclusions from PDA3E and PICH70A samples are generally devitrified or partially crystallized (Figure 3a), which indicates that they have cooled slowly. They display rounded or ovoid shapes and their size ranges from 10 to 40 μm for the Pichincha inclusions, and from 15 to 80 μm for the Pan de Azucar inclusions. They often contain, in addition to the glass, (1) a rim of host olivine that crystallized on the inclusion walls, (2) a gas bubble formed during thermal retraction, (3) ''daughter'' minerals that result from postentrapment crystallization of the trapped melt, (4) a preexisting spinel crystal included during inclusion formation, which never dissolves during experimental heating of the inclusions and also occurs as an isolated phase inside the olivine, and (5) some sulfide blebs (Figure 3).

4. Methods

4.1. Selection, Preparation, and Experimental Heating of the Melt Inclusions

[11] Several decimeter-size pieces of lavas were first crushed, and the 0.4–1.5 mm fraction was separated. Then, for each sample, about 800 olivine crystals were handpicked under a binocular microscope, glued on glass slides, and polished (silicon carbide paper and polishing disc with diamond solution, down to 1/4 μm). All the olivines have been studied under the microscope and only the unaltered and prismatic crystals were selected for the melt inclusion study, in order to avoid olivine crystals showing rapid-growth skeletal or dendritic morphologies, which may contain melt inclusions that sampled small volumes of the compositional boundary layer and therefore do not give direct information on the parental melt of the host crystal [*Faure and Schiano*, 2005]. Only the well-preserved primary melt inclusions, randomly distributed throughout the crystal and showing no cracks or links to the outside, were kept. This reduced the number of inclusions to about 100. This selection is the first step to ensure studying primary melt inclusions in equilibrium with the host olivine [*Faure and Schiano*, 2005].

[12] Before analysis, most of the selected melt inclusions were experimentally heated (indicated as the subscript ''H'' in Tables 1 to 3) in a Vernadsky-type microscope heating stage, which enables direct visual observation of the melting phenomena during the heating run. Heating experiments aim to reverse the processes that occurred inside the inclusions during natural cooling, such as formation of a bubble or crystallization of ''daughter'' minerals. During the experiments (at 1 atm), the oxygen fugacity was kept between 10^{-10} and 10^{-9} atm with He purified with Zr at 700°C, in order to avoid oxidation of the host mineral and to improve the cooling rate during quenching. Experiments were run at various heating rates and exposure times in order to assess the effects caused by variations in the rate of the transformations in the inclusions. The optimal experimental conditions ensuring equilibration during heating correspond to successive heating rates

Table 1 (Sample). Major Element Compositions of Primitive Olivine-Hosted Inclusions From Pichincha and Pan de Azucar Volcanoes[a] [The full Table 1 is available in the HTML version of this article at http://www.g-cubed.org]

	Pichincha																						
Inclusion	$A3a_H$	$A3c_H$	$J8_H$	$M3a_H$	$M3b_H$	A_H	B_H	C_H	$C2_H$	$D5a_H$	$L2_H$	$D5b_H$	$D1_H$	$F6_H$	CV_H	$5E3_H$	$MA02_H$	$MA03a_H$	$MA03b_H$	$MA04_H$	$MA05_H$	$MA5_H$	$MA6_H$
SiO_2	45.55	46.09	45.15	46.38	47.15	47.08	47.01	46.65	47.37	46.12	46.18	45.56	46.19	45.36	46.52	46.60	47.73	46.83	45.74	45.60	46.88	47.11	47.61
TiO_2	0.83	0.85	0.78	0.81	0.85	0.89	0.79	0.85	0.86	0.84	0.83	0.87	0.78	0.84	0.85	0.86	0.84	0.87	0.79	0.84	0.84	0.89	0.85
Al_2O_3	19.74	19.61	18.58	19.54	20.24	19.99	19.80	19.86	20.27	19.78	19.69	19.51	19.66	19.97	20.33	19.59	18.99	19.69	18.31	19.37	19.48	20.27	19.87
FeO_t	6.80	6.42	7.50	6.85	6.69	6.05	6.51	7.08	6.32	7.35	7.16	7.54	7.34	7.06	7.37	6.90	6.61	6.58	7.26	7.66	7.14	6.55	6.43
MnO	0.06	0.08	0.14	0.19	0.10	0.10	0.15	0.11	0.14	0.08	0.12	0.18	0.07	0.14	0.13	0.09	NA	NA	NA	NA	NA	NA	NA
MgO	7.74	7.40	9.07	8.18	7.67	7.19	7.21	7.18	7.28	7.95	6.53	7.95	8.12	8.40	7.38	8.01	8.11	7.67	8.11	8.48	8.23	7.09	7.81
CaO	12.82	13.31	12.16	12.55	13.01	13.10	12.72	13.33	12.96	12.55	12.21	12.80	12.27	13.11	12.84	13.41	13.53	13.20	12.52	13.12	12.90	13.61	13.36
Na_2O	3.33	3.66	3.04	3.21	3.25	3.69	3.53	3.60	3.66	3.34	3.44	3.19	3.34	3.21	3.47	3.27	3.38	3.37	3.24	3.39	3.47	3.49	3.53
K_2O	0.83	0.84	0.78	0.84	0.86	0.93	0.96	0.83	0.96	0.89	0.93	0.82	0.92	0.81	0.87	0.78	0.82	0.81	0.75	0.82	0.84	0.89	0.87
P_2O_5	0.19	<dl	0.15	0.16	0.18	0.17	0.14	0.15	0.20	0.13	0.18	0.15	0.13	0.14	<dl	0.13	0.20	0.15	0.14	0.15	0.16	0.16	0.15
Total	98.51	98.48	97.49	99.06	100.32	99.43	99.07	99.90	100.27	99.18	98.10	98.63	99.01	99.17	99.76	99.90	100.20	100.19	97.09	99.43	100.19	100.34	100.48
T_H	1231	1231	1215	1256	1256	1225	1253	1251	1251	1253	1181	1253	1244	1265	1236	1216	1210	1208	1208	1220	1236	1195	1251
$Mg^{\#}_{ol}$	88.10	88.10	88.33	88.19	88.19	87.73	87.43	88.41	88.41	87.52	86.93	87.52	87.72	87.76	87.79	88.32	88.06	88.68	88.68	88.10	87.79	88.25	89.08
$Mg^{\#}_{incl}$	69.27	69.54	70.55	70.28	69.43	70.18	68.69	66.76	69.53	68.19	64.36	67.61	68.67	70.22	66.50	69.71	70.85	69.77	68.89	68.69	69.52	68.16	70.65
K_D	0.30	0.31	0.32	0.32	0.30	0.33	0.32	0.26	0.30	0.31	0.27	0.30	0.31	0.33	0.28	0.30	0.33	0.29	0.28	0.30	0.32	0.29	0.25
X								2															3

[a] Major element compositions are given in wt%. The subscript "H" refers to experimentally heated melt inclusions. T_H is the temperature of disappearance of the last daughter minerals during the heating step. K_D is the value of the Fe/Mg exchange coefficient between the host olivine and its inclusion before the correction for post-entrapment olivine overgrowth. X is the percent of host-olivine dissolved in the inclusion during correction for post-entrapment olivine overgrowth. In these cases, the major element compositions given are the corrected values. $Mg^{\#}_{ol}$ is the molar ratio $Mg/(Mg+Fe) \times 100$ in the host olivine. $Mg^{\#}_{incl}$ is the molar ratio $Mg/(Mg + Fe^{2+}) \times 100$ in the inclusion. FeO_t is the total iron as FeO. <dl is inferior to detection level, and NA is not analyzed. Asterisk refers to whole rocks from *Bourdon et al.* [2003], Bourdon, personal communication (2007) and *Hoffer* [2008]. Here, total iron is given in Fe_2O_3. See references for analytical technique details.

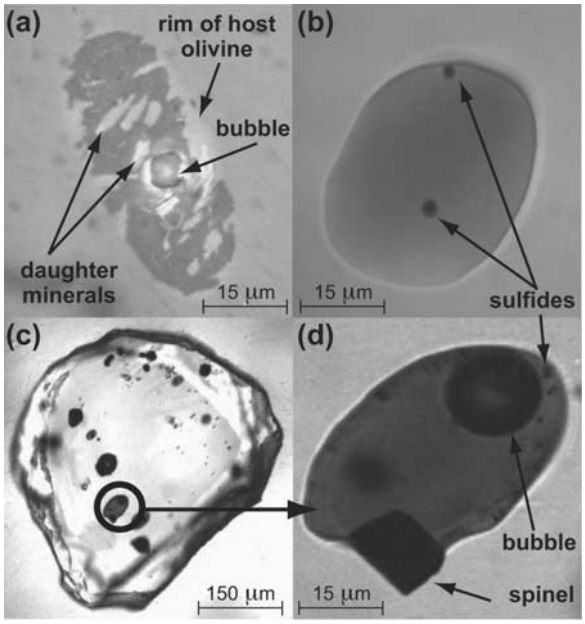

Figure 3. Photomicrographs of olivine-hosted melt inclusions from PDA3E sample. (a) Reflected-light photomicrograph of a melt inclusion before heating, with a rim of host olivine, daughter minerals and a bubble. (b) Glassy melt inclusion after heating, containing two small sulfide blebs. (c) Low-magnification photomicrograph showing an olivine grain with melt inclusions. (d) Enlargement of the marked area on Figure 3c, showing a melt inclusion after heating, containing a gas bubble formed during thermal retraction, a preexisting spinel crystal included during the formation of the inclusion, and some sulfide blebs.

of 0.4°C/s during 20 min, 0.3°C/s during 20 min, 0.2°C/s during 20 min, 0.1°C/s during 20 min, 0.05°C/s until the last "daughter" mineral has molten, and 10 additional minutes at temperature before quenching. The temperature was measured with a $Pt_{90}Rh_{10}$ thermocouple welded to the sample holder and calibrated with small grains of gold and silver, with melting points of 962°C and 1064°C, respectively. The accuracy of the temperature was better than 15°C at the maximum temperature. As the thermal retraction bubble did not disappear during the runs, the melt inclusions have only been heated up to the temperature of disappearance of the last daughter mineral (indicated as "T_H" in Table 1). The persistence of the bubble inside the inclusions during the heating experiments is likely to reflect that melt inclusions do not behave as purely isochoric systems during heating. Because of the inelastic behavior of the olivine, the difference between the initial pressure of trapping and the internal pressure of the inclusions at high temperature [*Schiano and Bourdon*, 1999] prevents a complete homogenization. After heating and quenching, the crystals were mounted on a 5 mm diameter brass mount filled with epoxy and the mounts were polished on silicon carbide paper to expose the melt inclusions. Final polish (down to 1/4 μm) was done with diamond solution after which the mounts were washed and put in ultrasound for 10 min first in purified alcohol, then in distilled water.

4.2. Microanalytical Techniques

4.2.1. Major Elements

[13] Major element compositions of olivine crystals and melt inclusions were obtained at the Laboratoire Magmas et Volcans (Clermont-Ferrand, France) using a Cameca SX 100 electron microprobe. We used a 15 kV accelerating voltage, a 15 nA current, and a focused beam for the olivine analyses. For glasses, the electron beam current was lowered to 8 nA and the beam was defocused to a size between 5 and 20 μm, depending on the diameter of the inclusion. A set of Cameca standards (natural and synthetic minerals and oxides) and natural glasses was used for calibration and instrumental stability monitoring. The counting times for glasses were Si, Fe, K: (40 s); Mn, Mg: (30 s); Ti, Al: (20 s); Ca, Na, P: (10 s). Typical relative analytical uncertainties obtained from replicate measurements of the Kilauea basaltic glass VG-A99 standard [*Jarosewich et al.*, 1979] were less than 2% for SiO_2, MgO, and Al_2O_3; 3.5% for FeO and CaO; 5% for K_2O, TiO_2, and Na_2O; 10% for P_2O_5; and 30% for MnO (1σ, c.f. Appendix A). No effect of alkali loss was observed on the natural basaltic glass standard under these conditions. We also checked that defocusing the beam did not affect the reproducibility by comparing analyses performed with a 5, 10, and 20 μm beam inside a single melt inclusion. Finally, the biggest inclusions were analyzed twice or more. The reproducibility for the measured elements was within the analytical errors (<2% for all oxides, except for P_2O_5, <5%, and MnO, <15%).

4.2.2. Trace Elements

[14] Trace element analyses were carried out at the Centre de Recherches Pétrographiques et Géochimiques (Nancy, France) using a Cameca IMS3f ion probe. The epoxy mounts were gold-coated. We used a 10 kV accelerating voltage of O^- primary beam with a 15 nA intensity, a 4.5 kV secondary accelerating voltage, a −80 V offset, a mass resolving power of 300, and a projected beam size

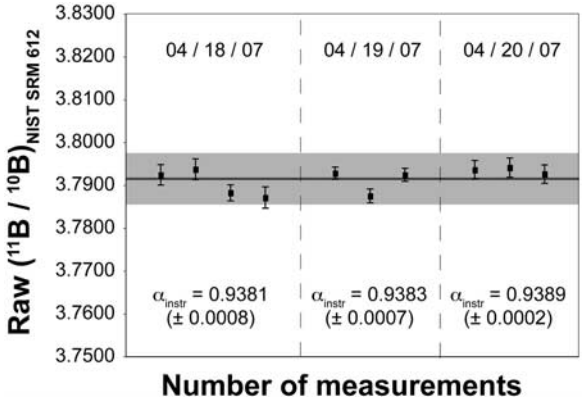

Figure 4. Reproducibility of the $^{11}B/^{10}B$ measurements of NIST SRM 612 standard glass. The values measured over the analytical session yield an overall standard deviation of ±0.0054 (2σ, gray bar) and an average error of ±0.0025 ($\sigma/\sqrt{n}$, 1σ error of mean, n = number of cycles). α_{instr} is calculated from the average of $^{11}B/^{10}B$ values over each day, relative to the NIST 612 standard value (average $^{11}B/^{10}B$ = 4.04039 ± 0.0299, according to a compilation by *Rosner et al.* [2008]). The error given on α_{instr} is the relative standard deviation (1σ) over the day.

between 20 and 30 μm. Each analysis consists of 15 cycles starting from 10.5 mass (used as background and for magnet adjustment), then ^{11}B(10 s), ^{30}Si (3 s), ^{88}Sr (5 s), ^{89}Y (5 s), ^{93}Nb (5 s), ^{96}Zr (8 s), and almost all the rare earth isotopes (10 s) (counting time in parenthesis). The data were corrected for oxide interferences [e.g., *Fahey et al.*, 1987]. We used the basaltic reference glasses KL2-G and ML3B-G [*Jochum et al.*, 2006] to control and correct the instrumental drift, and for the deconvolution procedure, to calculate the concentration of the elements in the samples (reference mass is ^{30}Si). Typical error on the samples (1 sigma error of mean: $\sigma/\sqrt{n}$, n = number of cycles) is less than 10% for all trace elements, except for La, Nd, Yb, Lu (<15%), and Eu (<17%).

4.2.3. Boron Isotopes

[15] Boron isotopes were analyzed at Woods Hole Oceanographic Institution (Massachusetts, USA) using a CAMECA 1280 ion probe. Samples were first mounted in epoxy and polished in order to carry out major and trace elements analyses. As epoxy can contain significant amounts of boron that would increase the background signal during boron isotopic analysis, the grains were removed from the epoxy mounts using a soldering iron, then they were pressed into a high-purified indium mount, put in ultrasound in pure ethanol followed by distilled water, and then gold-coated. A primary beam of 7nA of O_2^- was delivered onto the sample with a nominal accelerating voltage of 12.5 kV. The secondary ion accelerating voltage was 10 kV, and the final impact energy was thus 22.5 kV. The mass resolution was set at 2450, high enough to separate isobaric interferences (the interference of mass $^{10}B^1H$ on mass ^{11}B is resolved with a resolution power higher than 1416, and the interference of mass $^1H^9Be$ on mass ^{10}B is resolved with a resolution power higher than 962). A critical illumination focusing was used. The size of the contrast aperture was 400 μm and that of the field aperture was 3000 μm. The energy window, which was initially centered on the optimized position for the ions, was opened to allow ions with a range of 50 eV into the mass spectrometer. No energy filtering was used. The samples were first presputtered for 2 min to remove surface contaminants and then analyses were performed with a projected beam size between 20 and 30 μm. Each analysis was composed of 50 cycles: 9.3 (background, 3 s), ^{10}B (3 s waiting time, 20 s analysis), and ^{11}B (2 s waiting time, 10 s analysis). Typical ^{10}B intensity measured in the samples was 1×10^3 cps, down to rare minimum of 4×10^2 cps. For each analysis we monitored the peak intensity and the stability of the $^{11}B/^{10}B$ ratio. The instrumental fractionation ($\alpha_{instr} = \frac{(^{11}B/^{10}B)_{measured}}{(^{11}B/^{10}B)_{true}}$) was assessed by daily measurements of the NIST 612 standard (average composition of $^{11}B/^{10}B$ = 4.04039 ± 0.00299, according to a compilation of MC-ICPMS, TIMS, and SIMS data by *Rosner et al.* [2008]). One day was dedicated to the instrumental tuning and stabilization of the magnet. Reproducibility on this standard over the 3 days of sample analysis is presented on Figure 4. The $^{11}B/^{10}B$ values of the standard measured over our analytical session yields an error of less than 0.0025 (1σ error of mean: $\sigma/\sqrt{n}$, where n is number of cycles). After correction for instrumental mass fractionation, boron isotopes in the samples are expressed in δ^{11}B ($\delta^{11}B = \left[\frac{(^{11}B/^{10}B_{measured})/\alpha_{instr}}{^{11}B/^{10}B_{reference}} - 1\right] \times 1000$, Table 3) relative to NIST SRM 951 ($^{11}B/^{10}B$ = 4.04558 ± 0.00035 [*Palmer and Slack*, 1989]). We applied a signal drift correction scheme (data processing after acquisition with a Matlab program, doubly interpolated ratios variable in time (K. Koga, personal communication, 2008)). This led to an error reduction by 30% while keeping the same δ^{11}B (Table 3).

Table 2. Trace Element Compositions of Primitive Olivine-Hosted Inclusions From Pichincha and Pan de Azucar Volcanoes[a]

	Pichincha						Pan de Azucar												
Inclusion	$M3a_H$	$D1_H$	**$MA03a_H$**	$MA5_H$	**MC01**	**MA01a**	3.1	3.8	**7.7**	3.3	**$H3a_H$**	$D6b_H$	**$K9_H$**	Aa_H	**$D1a_H$**	4.2	5.5	Whole Pda3E	Rocks* Pich70A
$Mg_{ol}^{\#}$	88.19	87.72	88.68	88.25	86.15	87.42	87.35	88.45	88.04	87.58	81.82	80.10	80.07	78.98	81.48	81.97	78.24		
B	<dl	8.7	12.2	7.7	7.8	7.3	5.3	7.0	8.3	14.3	7.1	<dl	6.2	7.4	5.6	7.1	8.1	4.8	13.6
Sr	355.0	293.9	322.0	262.5	252.1	160.1	296.6	180.7	197.2	426.6	1333.7	1420.0	1239.5	1543.6	936.4	1254.2	1814.4	1150.0	390.0
Y	14.0	9.9	13.3	9.7	12.2	6.3	11.6	18.4	14.1	7.7	24.2	29.0	21.5	24.1	13.2	34.6	24.1	211.0	14.5
Zr	67.0	47.1	51.0	36.1	65.2	26.8	37.9	95.9	51.9	34.7	122.8	143.8	92.4	114.1	68.4	203.1	123.8	88.0	70.0
Nb	0.7	1.2	1.3	1.1	1.5	0.7	<dl	1.4	1.2	1.2	18.0	<ld	11.4	19.1	11.6	17.8	31.6	11.5	2.1
Ba	306	285	262	230	136	142	233	130	180	392	948	1142	950	1186	719	717	1394	840	427
La	5.02	4.44	4.12	3.18	2.47	1.65	2.83	3.38	3.52	4.15	37.56	41.89	38.55	44.33	25.28	32.48	48.80	27.50	10.30
Ce	10.97	9.60	9.44	5.98	5.12	4.13	6.29	8.35	9.50	7.90	69.56	83.47	76.91	86.64	44.57	69.49	94.35	53.50	15.00
Pr	1.62	1.36	1.26	0.89	0.89	0.67	0.93	1.44	1.36	0.98	8.83	11.81	9.27	10.45	6.07	9.96	12.46	NA	NA
Nd	8.01	6.09	6.05	3.85	4.75	2.83	4.64	8.03	7.02	4.49	32.43	53.46	37.82	42.64	20.41	50.56	52.72	30.50	11.20
Sm	2.10	1.53	1.82	1.10	1.23	1.03	1.21	2.34	2.05	1.12	6.53	11.59	7.87	8.56	5.19	10.96	10.51	6.25	2.4
Eu	0.63	NA	NA	0.29	NA	0.22	0.44	NA	0.74	NA	1.99	3.83	2.17	2.49	1.38	3.97	2.97	1.84	0.75
Gd	NA	2.34	2.40	NA	1.09	0.80	1.23	2.04	2.27	NA	NA	NA	NA	NA	NA	NA	NA	5.20	2.70
Dy	2.66	1.81	2.22	1.12	1.44	0.98	1.32	2.43	2.26	1.34	4.84	8.53	5.69	6.27	3.47	8.09	7.80	3.80	2.50
Er	1.44	1.03	1.14	0.83	0.96	0.52	0.71	1.28	1.23	0.81	2.73	3.53	2.54	2.93	1.75	3.48	3.35	1.80	1.40
Yb	1.37	0.84	1.17	0.70	0.80	0.55	0.72	1.35	1.27	0.84	1.79	2.73	1.97	2.48	1.19	2.83	2.31	1.53	1.35
Lu	0.25	0.18	0.15	0.07	0.12	0.08	0.09	0.22	0.18	0.13	0.24	0.35	0.28	0.24	0.16	0.35	0.31	NA	NA

[a] Trace element compositions are given in ppm. The subscript "H" refers to experimentally heated melt inclusions. $Mg_{ol}^{\#}$ is the molar ratio Mg/(Mg + Fe)*100 in the host olivine. Asterisk refers to whole rocks from *Hoffer* [2008], *Bourdon et al.* [2003], and E. Bourdon (personal communication, 2007). Inclusions that were analyzed for both trace elements and B isotopes are in boldface.

Table 3. Boron Isotope Compositions of Primitive Olivine-Hosted Melt Inclusions From Pichincha and Pan de Azucar Volcanoes[a]

Inclusions	$Mg_{ol}^{\#}$	$\delta^{11}B_{corr}$	σ_m
	Pichincha		
$M3b_H$	88.19	−9.4	2.9
$A3a_H$	88.10	−0.3	1.0
$L2_H$	86.93	+3.5	1.4
$MC2_H$	88.24	−8.1	0.9
MC1	86.98	−1.2	0.9
$MA6_H$	89.08	−2.3	1.4
$MC04_H$	87.70	−7.3	1.1
MC01	86.15	+3.5	1.6
$MA03a_H$	88.68	−8.4	1.1
MA01a	87.42	−9.5	1.3
7.7	88.04	+2.8	0.8
3.2	88.83	−2.1	2.2
3.5	87.84	+0.0	2.4
	Pan de Azucar		
L2	80.88	−2.8	1.5
L14	78.92	−5.8	0.8
L3	84.02	−14.2	1.8
$C2_H$	79.16	−7.1	1.1
$D1a_H$	81.48	−10.8	1.2
$A1a_H$	88.10	−13.0	2.3
$K9_H$	80.07	−13.0	1.1
9B5	81.73	−3.0	1.0
L12	84.52	−9.8	1.2
$E2a_H$	78.25	−13.0	1.1
L12-2	84.52	−9.7	1.2
$H3a_H$	81.82	−17.9	0.8
L11	79.67	−6.9	0.5
$6K8a_H$	78.18	−1.9	1.4
10C3	81.73	−6.8	1.0
$5A5_H$	79.05	−6.3	1.1
$10H2_H$	85.37	−12.3	2.4
5.3	86.38	−4.9	1.0
4.4	88.42	−7.0	2.4
4.7	85.02	−5.7	2.3
4.3	87.10	−5.9	2.4

[a] Boron isotope compositions are given in ‰. The subscript "H" refers to experimentally heated melt inclusions and $\sigma_m = \sigma/\sqrt{n}$, where n is the number of analytical cycles. Each line represents a single point measurement. Inclusions that were analyzed for both trace elements and B isotopes are in boldface. The variable $\delta^{11}B_{corr}$ indicates that all the $^{11}B/^{10}B$ raw data were corrected for the matrix effect on NIST SRM 612 according to *Rosner et al.* [2008], i.e., shifted by 0.01375 toward lower values. See text for details.

[16] A recent study by *Rosner et al.* [2008] pointed out, for the first time, the discrepancy that exists between the NIST 610, 612, and 614 and other standard glasses mainly coming from the study of *Jochum et al.* [2006]. On the basis of a compilation of MC-ICPMS, TIMS, and SIMS data from the literature, *Rosner et al.* [2008] reported an average shift in $\delta^{11}B$ of −3.4‰ between NIST standards and the others, which corresponds to a shift on $^{11}B/^{10}B$ of 0.01375 toward lower values. Since we used NIST 612 as a standard, we needed to correct the $^{11}B/^{10}B$ data from this shift. However, there is no consensus on how to correct the $^{11}B/^{10}B$ values obtain relative to NIST standard yet. Although this shift has been observed and quantified on other ion probes (A. Shaw and A. Gurenko, personal communication, 2008; E. Rose-Koga and K. Koga, personal communication, 2008), none of those results are published yet. The position we took is to correct the data with the only published value, i.e., the shift of 0.01375 from *Rosner et al.* [2008]. The values corrected from the shift are reported in Table 3 (expressed in $\delta^{11}B_{corr}$).

5. Results

[17] Major elements were measured in all experimentally heated inclusions (Table 1). Trace elements and boron isotope compositions were measured in the biggest melt inclusions (Tables 2 and 3). Although we measured the trace element concentrations in 17 melt inclusions and the $\delta^{11}B$ compositions in 34 melt inclusions, we succeeded in analyzing both trace elements and boron isotopes in only 7 inclusions (melt inclusions in boldface, Tables 2 and 3), as most of the inclusions were less than 40 μm in diameter and SIMS analyses are destructive.

[18] A few rare melt inclusions contained only small crystals as dendritic aggregates. As the glassy area was large enough to allow SIMS analyses, we did not heat them. In this case, the entire surface of the inclusions was rastered during the ion probe analysis, in order to average the signal of both the glass and the crystals. We controlled carefully that no significant difference exists between the heated inclusions and the non-heated melt inclusions by comparing the trace elements patterns of the two types of inclusions.

5.1. Equilibrium Between the Melt Inclusions and Their Host Olivines

[19] To test the equilibrium between the trapped melts and their host olivine crystals, we calculate the expected value for the Mg/Fe exchange coefficient between olivine and liquid, $K_{Dol\text{-}melt}^{Mg\text{-}Fe}(K_D)$, using the model proposed by *Toplis* [2005], which accounts for the effects of pressure, temperature, olivine, and liquid compositions. Fe^{3+}/Fe^* was estimated using the experimentally calibrated relation from *Kilinc et al.* [1983]. This relation requires the f_{O_2} calculation, which was estimated by the determination of the sulfur speciation in the glass

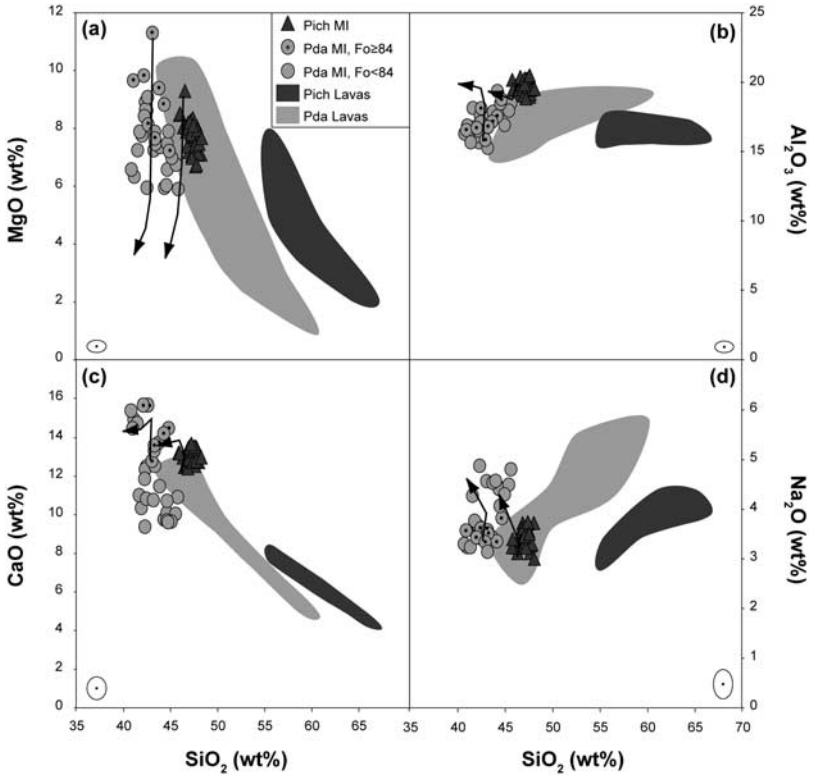

Figure 5. SiO_2 variations as a function of (a) MgO, (b) Al_2O_3, (c) CaO, and (d) Na_2O in melt inclusions trapped in the olivine phenocrysts from Pichincha (Pich) and Pan de Azucar (Pda) samples (triangles and circles, respectively), compared with the compositional fields for the whole rocks [*Bourdon et al.*, 2003; *Hoffer*, 2008]. The circles with a dot in the middle represent Pan de Azucar melt inclusions in olivines with forsterite content (Fo) higher than 84%. The black arrows correspond to the liquid lines of descent calculated using the Hbasalt phase equilibrium model from *Weaver and Langmuir* [1990] (updated version is *Langmuir et al.* [2006]), starting from one of the most primitive melt inclusions of each volcano, using a pressure of 0.5 GPa and an estimated water content of 2 wt%. They indicate that the melt inclusions cannot be simply considered as parental magmas evolving toward the compositions of whole rocks by fractional crystallization. All major elements compositions have been recalculated to 100% on a volatile-free basis. The four white ellipses, at the corner of each graph, represent the values of maximum errors ($\pm 1\sigma$).

of the inclusions from the measurement of the peak shift of the sulfur K_α radiation relative to a sulfide standard with the electron microprobe [*Jugo et al.*, 2005]. The calculations showed that, within the analytical errors on the FeO and MgO concentrations, the value of $K_D = 0.30 \pm 0.03$ is appropriate to the studied liquids. Most of the heated inclusions have calculated $K_D^{Mg\text{-}Fe}$ values consistent with the nominal value of 0.30 ± 0.03, indicating that they are unlikely to have suffered from reequilibration processes that generally result in lower FeO and higher MgO contents and thus higher $K_D^{Mg\text{-}Fe}$ values in the inclusions [*Danyushevsky et al.*, 2000]. However, some heated inclusions show low $K_D^{Mg\text{-}Fe}$ values (14 inclusions have $K_D^{Mg\text{-}Fe}$ between 0.19 and 0.26, Table 1), which indicate that even if all the "daughter" minerals disappeared during the heating step, the olivine rim on the inclusion wall has not been completely melted. These inclusions have required a correction for postentrapment olivine overgrowth at the inclusion wall by numerically dissolving increments of olivine into the liquid until the $K_D^{Mg\text{-}Fe}$ reaches the equilibrium value, following the procedure by *Laubier et al.* [2007]. The amount of olivine dissolved into the melt, indicated as "X" in Table 1, is always less than 12%.

5.2. Major Elements

[20] Olivine (Fo_{83-89})-hosted melt inclusions from Pichincha display a limited range of compositions. They contain between 45.2 and 47.9 wt% SiO_2, 6.5–9.1 wt% MgO, 18.3–20.4 wt% Al_2O_3, 12.2–13.6 wt% CaO (Table 1; Figure 5), and their Mg# (defined as $Mg/(Mg + Fe^{2+}) \times 100$) range from 64.4 to 70.9% (Table 1). Their compositions are all nepheline-normative, with normative nepheline

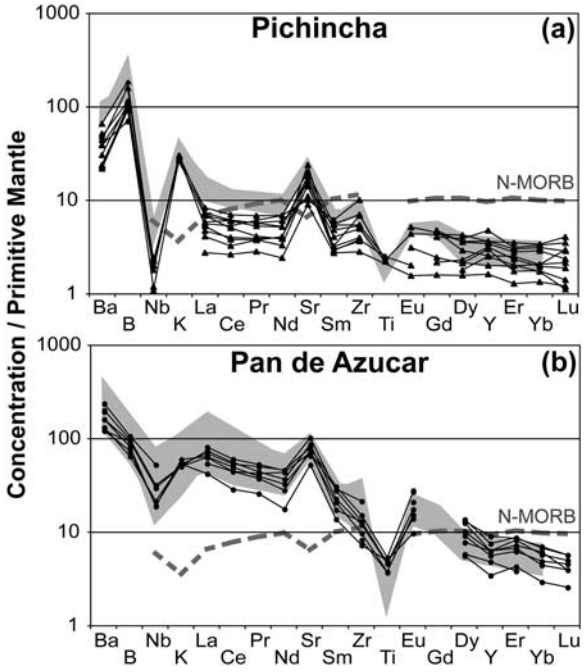

Figure 6. Primitive mantle-normalized spidergram for melt inclusions (black lines) and whole rocks (shaded area) [*Bourdon et al.*, 2003; *Hoffer*, 2008] from (a) Pichincha and (b) Pan de Azucar. The incompatibility order and normalizing values are from *Hofmann* [1988]. The dashed line is the average N-MORB composition of *Hofmann* [1988] shown for comparison.

contents varying between 5.4 and 13.3%. The comparison between Pichincha melt inclusions and whole rocks is illustrated by the SiO_2 variation diagrams of Figure 5. The melt inclusions fall on a continuous extension of the trend defined by the whole rocks, but they are separated from them by a 7 wt% SiO_2-gap in the MgO and CaO versus SiO_2 diagrams (Figures 5a and 5c). However, they do not fall on a continuous extension of the trend defined by the whole rocks in the Na_2O and Al_2O_3 versus SiO_2 diagrams (Figures 5b and 5d); the melt inclusions define a population offset toward lower SiO_2, but also toward higher Na_2O and Al_2O_3 contents from the whole rock trend.

[21] Olivine (Fo_{74-88})-hosted melt inclusions from Pan de Azucar have nepheline-normative compositions (from 12.9 to 22.4%) characterized by variable contents of SiO_2 (39.8–45.6 wt%), MgO (5.6–11.2 wt%), Al_2O_3 (14.9–19.2 wt%), and CaO (9.3–15.4 wt%; Table 1, Figure 5). Their $Mg^{\#}$ values vary between 47.8 to 69.5% (Table 1). In Figure 5, they plot at the lowest SiO_2 end of the bulk rock trends; however, they clearly define a different array of compositions from that of the whole-rock compositions and extend toward lower CaO and higher Na_2O contents at a given SiO_2 content (Figures 5c and 5d).

5.3. Trace Elements

[22] Trace element analyses of the melt inclusions from Pichincha and Pan de Azucar are reported in Table 2 and illustrated in primitive mantle-normalized trace element diagrams (Figure 6), together with the bulk-rock compositions of lavas [*Bourdon et al.*, 2003; *Hoffer*, 2008] and the average N-MORB composition [*Hofmann*, 1988]. All the melt inclusions display trace element patterns that are typical of arc magmas: they are enriched in large-ion lithophile elements (LILE; Ba, K, and Sr) and depleted in Nb and Ti (high-field strength elements; HFSE). They are also depleted in heavy rare earth elements (HREE) relative to MORB and enriched in light rare earth elements (LREE) relative to HREE. These trace element features are believed to result from melting of mantle sources initially slightly depleted with respect to the sources of N-MORB, then metasomatized by slab-derived, H_2O-rich phases segregating mobile from nonmobile elements [e.g., *Gill*, 1981; *Tatsumi and Eggins*, 1995].

[23] In detail, however, the trace element patterns for Pichincha melt inclusions are flatter (La/Yb = 2.5–5.3, Figure 6a) compared with the Pan de Azucar inclusions (La/Yb = 11.5 to 21.2, Figure 6b). The negative Nb anomaly is more significant for Pichincha melt inclusions (Nb/Nb* of 0.005 on average) than for Pan de Azucar melt inclusions (Nb/Nb* of 0.05 on average). They also show small Zr and Y positive anomalies whereas small negative anomalies for these two elements are observed in the Pan de Azucar melt inclusions.

[24] For the two volcanoes, the melt inclusions and bulk lavas display similar trace element patterns. However, if the compositional range of the trapped melts within Pan de Azucar melt inclusions is almost as large as the whole range for bulk rocks (Figure 6b), the trace elements concentrations in Pichincha melt inclusions are often lower than that for the whole rocks (Figure 6a) and their dispersion largely exceeds that for the bulk rocks (Figure 6a). This dispersion could at first glance reflect an effect of dilution by the host olivine. Owing to the smaller size of the Pichincha melt inclusions, the beam of the ion probe could have ablated a small amount of host olivine on the edge of or beneath the melt inclusions during the trace element analyses. An alternative hypothesis is that the dispersion reflects an effective heterogeneity in the

compositions of the trapped primitive magmas. This is supported by the variation of very incompatible element ratios such as Ba/La, which ranges from 39 to 95 for the Pichincha melt inclusions. Accordingly, several studies have revealed that primitive melt inclusions display more variable compositions than their host bulk rocks [e.g., *Sobolev and Shimizu*, 1993; *Gurenko and Chaussidon*, 1995; *Saal et al.*, 1998; *Schiano et al.*, 2000]. In these cases, melt inclusions have been interpreted as melts reflecting a range of source compositions and/or extents of melting, and trapped before mixing processes in magma chambers where they were mixed to produce the compositions of erupted lavas.

5.4. Boron Concentrations and Boron Isotope Compositions

[25] Boron concentrations (in ppm) and boron isotope compositions (δ^{11}B, in ‰) in the melt inclusions are given in Tables 3 and 4. Boron concentrations range from 5.3 to 14.3 ppm for Pichincha melt inclusions and from 5.6 to 8.1 ppm for Pan de Azucar melt inclusions. They are consistent with typical arc lava values (e.g., 4–20 ppm) [*Leeman and Sisson*, 1996]. The correlations between the concentrations of boron and other elements are generally poor. Boron isotopic compositions of Pichincha melt inclusions span a large range of δ^{11}B values, from -9.5 ± 1.3‰ to $+3.5 \pm 1.4$‰. Pan de Azucar melt inclusions also display highly variable δ^{11}B, but the values are more negative, ranging from -17.9 ± 0.8‰ to $+1.9 \pm 1.4$‰. Boron isotope compositions for Pichincha and Pan de Azucar melt inclusions are in good agreement with the scarce data previously obtained for Ecuadorian whole rocks (averages of $+1.4 \pm 0.5$‰ for Pichincha whole rocks and -5.1 ± 0.5‰ for Sumaco whole rocks (E. Bourdon, personal communication, 2007)). In summary, the large range of δ^{11}B measured in the Pichincha and Pan de Azucar melt inclusions shows that the trapped melts could not simply derive from an unmetasomatized part of the mantle, and that consequently, one or several other reservoirs, with different δ^{11}B compositions, have to come into play.

6. Discussion

6.1. Relationship Between the Melt Inclusions and the Host Rocks

[26] Prior to discussing the compositions of the melt inclusions in terms of mantle source regions, it is important to assess the pristine character of the liquids trapped inside the olivine phenocrysts, their significance, and their relationship with their host lavas. Some of the studied melt inclusions, in particular those preserved in the magnesium-rich olivine crystals (Fo $\geq$ 84) have nepheline-normative compositions characterized by unusually high CaO concentrations relative to typical arc magmas ($\leq$13%) [e.g., *Schiano et al.*, 2000]. Such high CaO contents in primitive melt inclusions have previously been interpreted as the result of local disequilibrium due to localized fast crystallization rates [*Danyushevsky et al.*, 2004]. This hypothesis is, however, difficult to reconcile with the fact that the melt inclusions are in chemical equilibrium with their host olivines with respect to Fe and Mg, but also Ca (using partition coefficients from *Beattie* [1994] or *Gaetani and Grove* [1998]), and that melt inclusions trapped in polyhedral olivines only, a morphology which results from slow crystal growth [*Baronnet*, 1984] were selected. Therefore, although local disequilibrium remains a possible explanation for the high CaO concentrations of some melt inclusions, we will consider in the following discussion that the melt inclusions from Pichincha and Pan de Azucar contain small volumes of the parental liquids of their host olivines.

[27] Pichincha and Pan de Azucar melt inclusions trapped in magnesium-rich olivine phenocrysts cannot be simply considered as parental magmas evolving toward the compositions of whole rocks by fractional crystallization (Figure 5). First, in some of the variation diagrams, the melt inclusions do not fall on continuous extensions of the trends defined by the whole rocks (Figure 5). In addition, there is a significant compositional gap (maximum of 7 wt% for SiO_2) between Pichincha melt inclusions and its bulk lavas, which is unlikely to be accounted for by crystal fractionation. Liquid lines of descent calculated using the Hbasalt phase equilibrium model from *Weaver and Langmuir* [1990] (updated version of *Langmuir et al.* [2006]), starting from the most primitive melt inclusions of each volcano, evolve in the opposite direction from the whole rock trends (black arrows in Figure 5). Finally, mass balance calculations performed using the average compositions of the melt inclusions and the host lavas (Pich70A and Pda3E) as parental and daughter melts, and the phenocrysts and minor phases present in the host lavas as fractionating phases, do not give acceptable results. Thus, no clear relationship can be found between the melts trapped in the olivine phenocrysts and the erupted lavas. Our preferred

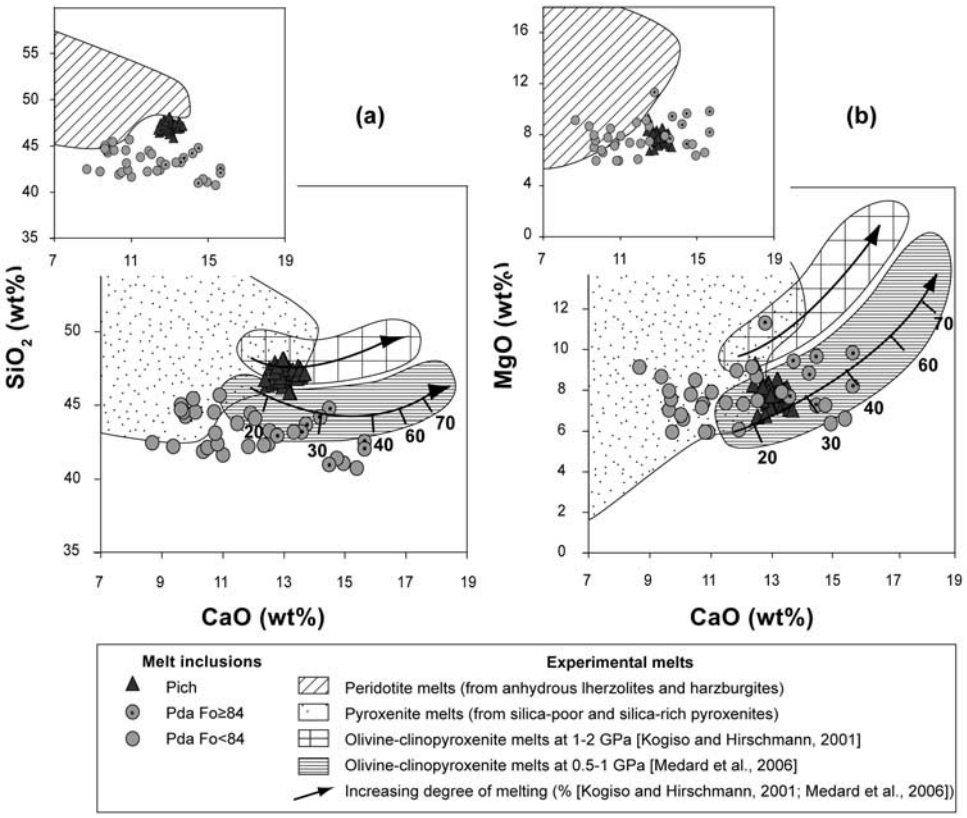

Figure 7. Plots of (a) SiO_2 and (b) MgO versus CaO concentrations, comparing melt inclusions from Pichincha (Pich) and Pan de Azucar (Pda) with experimental melts of pyroxenites at 0.5–5.0 GPa (dotted area) [*Ito and Kennedy*, 1974; *Kogiso et al.*, 1998; *Takahashi et al.*, 1998; *Kogiso et al.*, 2003; *Pertermann and Hirschmann*, 2003; *Keshav et al.*, 2004; *Kogiso and Hirschmann*, 2006], olivine clinopyroxenites at 0.5–1.0 GPa (horizontally striped area) [*Médard et al.*, 2006] and 1–2 GPa (squared area) [*Kogiso and Hirschmann*, 2001]. The arrows show the effect of a progressive increase in the degree of partial melting. Inserts show the comparison between the melt inclusions from Pichincha and Pan de Azucar and experimental melts of peridotites (hatched area; anhydrous lherzolites and harzburgites at 0.5–7 GPa) [*Hirose and Kushiro*, 1993; *Baker and Stolper*, 1994; *Baker et al.*, 1995; *Kushiro*, 1996; *Hirschmann et al.*, 1998; *Robinson et al.*, 1998; *Walter*, 1998; *Pickering-Witter and Johnston*, 2000; *Falloon et al.*, 2001; *Schwab and Johnston*, 2001; *Wasylenki et al.*, 2003]. All major elements compositions have been recalculated to 100% on a volatile-free basis.

explanation for this absence of relationship is that it reflects several combined effects of mixing of different melt batches and different degrees of fractional crystallization. Such a combination of processes is similar to what was proposed by *Schiano et al.* [2000, 2004] to explain the compositional variability in arc lavas from south Italy and Luzon (the Philippines) and their associated CaO-rich olivine-hosted melt inclusions.

[28] In the following discussion, we focus on the origin of the compositional characteristics of the trapped melts. In particular, two main features need to be addressed: (1) the melt inclusions preserved in magnesium-rich olivine crystals (Fo $\geq$ 84) from Pichincha and Pan de Azucar lavas define a population of primitive magmas (termed the CaO-rich primitive melt inclusion population hereafter) that is compositionally distinct from typical arc lavas. They are characterized by relatively high CaO, low SiO_2 contents and nepheline-normative compositions. This population consists of all the Pichincha melt inclusions (triangles in Figures 5 and 7) and a subset of the Pan de Azucar melt inclusions (circles with a dot in the middle in Figures 5 and 7); (2) melt inclusions from Pichincha have higher ratios of fluid-mobile over less fluid-mobile element ratios and more higher boron isotope values than melt inclusions from Pan de Azucar, indicating cross-arc variation of the slab contribution (Figure 8).

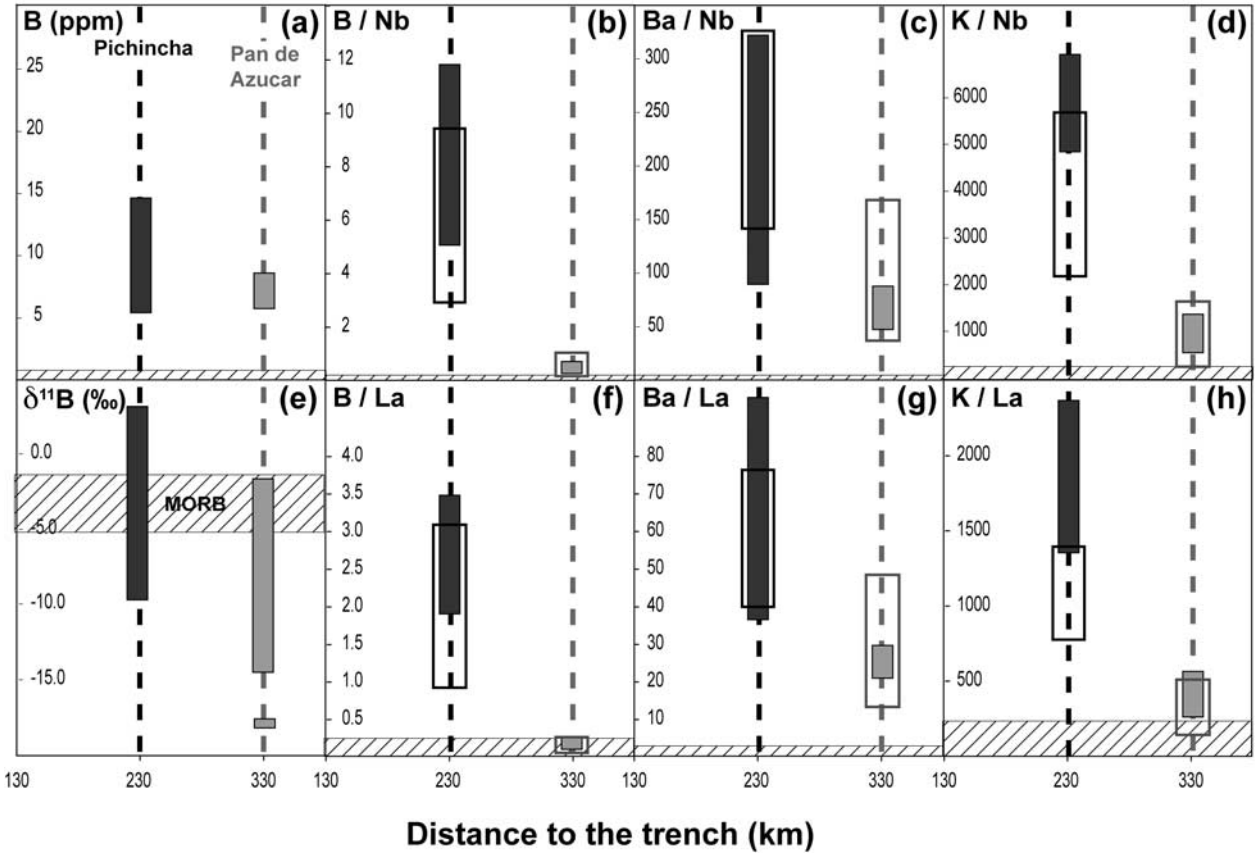

Figure 8. Variations in (a) B, (e) δ^{11}B, and (b, c, d) B, Ba and K over Nb or (f, g, h) La ratios with respect to the distance to the trench for melt inclusions (filled rectangles) and whole rocks from Pichincha and Pan de Azucar (open rectangles) [*Bourdon et al.*, 2003; *Hoffer*, 2008]. The hatched area represents MORB data from *Chaussidon and Marty* [1995] (Figures 8a and 8e) and *Hofmann* [1988] (Figures 8b–8d and Figures 8f–8h).

6.2. Nature of the Source of the CaO-Rich Primitive Melt Inclusion Population

[29] Arc lavas are generally believed to result from melting of depleted peridotitic lithologies previously enriched by an H_2O-rich phase released from the subducting slab [e.g., *Gill*, 1981; *Tatsumi and Eggins*, 1995]. However, this model cannot easily be reconciled with the chemical compositions of the CaO-rich primitive melt inclusions studied here. As argued in the work of *Schiano et al.* [2000], their SiO_2-undersaturated and CaO-rich character cannot be formed from partial melting of common peridotitic mantle as it strongly contrasts with experimental melts of lherzolite or harzburgite (inserts in Figure 7). In fact, nepheline-normative experimental melts could be generated by melting of a peridotitic lithology with increasing pressures of melting, but this evolution is associated with a decrease in the CaO content [e.g., *Green and Ringwood*, 1967; *O'Hara*, 1972]. Also, the maximum CaO content of the experimental liquids (~13 wt%) [*Hirose and Kushiro*, 1993; *Wasylenki*, 1998] produced by melting of anhydrous peridotites at degrees of melting required for clinopyroxene exhaustion (up to 25%) [e.g., *Schiano et al.*, 2000] is still below the highest values of CaO contents of the melt inclusions studied here. In addition, liquids produced at such a high degree of melting are not nepheline-normative. Melting of a peridotitic lithology under hydrous conditions produces SiO_2-rich liquids characterized by lower CaO contents than in the case of anhydrous melting [*Gaetani and Grove*, 1998; *Hirose and Kawamoto*, 1995]. Finally, melting of peridotite in the presence of CO_2 can generate nepheline-normative, CaO-rich melts [*Hirose*, 1997; *Dalton and Presnall*, 1998], but with lower SiO_2 and Al_2O_3 and much higher MgO concentrations than in the melt inclusions of this study.

[30] Source lithologies other than peridotites should thus be considered for the generation of

the CaO-rich primitive melt inclusion population. The various components that could potentially account for the geochemistry of Ecuadorian lavas are the mantle wedge, the subducting slab (i.e., the sediment cover and oceanic crust from the Carnegie ridge), and the South American lower continental crust. These components occur in three main lithologies: peridotites from the mantle, eclogites from the slab, and pyroxenites from the upper mantle or the lower crust.

[31] The presence of adakite-like lavas ascribed to slab melting has been reported in Ecuadorian volcanoes [e.g., *Bourdon et al.*, 2003; *Samaniego et al.*, 2005; *Hidalgo et al.*, 2007; *Hoffer et al.*, 2008]. Experimental results indicate that partial melting of subducted metabasalts may occur at the garnet amphibolite-eclogite transition [e.g., *Rapp et al.*, 1999]. However, this process generates relatively high SiO_2, high Al_2O_3, mostly quartz and corundum-normative melts. Consequently, melting of the subducted oceanic crust at moderate to high pressures is not a plausible explanation for the origin of the CaO-rich, silica-undersaturated melt inclusions.

[32] An alternative hypothesis is that these compositions result from the melting of clinopyroxene-rich lithologies, i.e., pyroxenites [*Schiano et al.*, 2000; *Kogiso et al.*, 2004; *Médard et al.*, 2006]. As illustrated by the CaO-variation diagrams in Figure 7, the compositions of the CaO-rich primitive melt inclusions are consistent with experimental melts of pyroxenite (see caption of Figure 7 for references). These include silica-saturated melts, but also silica-undersaturated melts produced by partial melting of silica-poor garnet pyroxenites at 0.5–5.0 GPa [*Hirschmann et al.*, 2003; *Kogiso et al.*, 2003, 2004; *Keshav et al.*, 2004] and olivine clinopyroxenites at 0.5–2.0 GPa [*Kogiso and Hirschmann*, 2001; *Médard et al.*, 2006]. Melting of a silica-deficient (relative to the garnet-pyroxene thermal divide) garnet pyroxenite can generate nepheline-normative melts [*O'Hara*, 1972; *Schiano et al.*, 2000; *Hirschmann and Pertermann*, 2000], whereas the silica-undersaturated character of melts produced from amphibole-bearing olivine clinopyroxenites mainly results from the breakdown of the pargasitic amphibole [*Médard et al.*, 2006]. The CaO-rich primitive melt inclusions represent intermediate to high degree partial melts of amphibole-bearing olivine clinopyroxenites formed at low to moderate pressures (Figure 7, from 20 to 40% of melting at 0.5–2 GPa) [*Médard et al.*, 2006; *Kogiso and Hirschmann*, 2001]. In this case, the source of the Pichincha and Pan de Azucar CaO-rich primitive melt inclusions must be found in the lower crust or upper mantle regions beneath exhumed volcanic arcs where these lithologies generally occur as zoned cumulate complexes [*Schiano et al.*, 2000, and references therein].

[33] Unlike Pichincha melt inclusions, which do not show a significant evolution, Pan de Azucar melt inclusions display a continuous change, illustrated by compositional trends in Figure 5. The decrease in the CaO, MgO, and TiO_2 contents is accompanied by an increase in the FeO, Na_2O, K_2O, and P_2O_5 contents. Progressive melting of an initially clinopyroxenite-rich lithology cannot simply explain this evolution because the CaO concentrations in partial melts of amphibole-bearing olivine clinopyroxenites increase with increasing degrees of melting (arrows in Figure 7) [*Médard et al.*, 2006]. The evolution by fractional crystallization was evaluated using least squares mass balance calculations for the major elements with Pan de Azucar phenocryst chemistry (olivine, clinopyroxene, opaque, plagioclase, amphibole, apatite) [*Hoffer*, 2008]. For the majority of the melt inclusions, mass balance calculations do not give acceptable results. It is thus considered unlikely that the compositional variations in the melt inclusions reflect a simple liquid line of descent. An alternative explanation for the compositional variation among the Pan de Azucar melt inclusions is that it records a mixing process between the most CaO-rich inclusions interpreted as melts of pyroxenite and "normal" melts of peridotite (inserts in Figure 7). Arguments for this hypothesis are the linear character of the melt inclusion correlations seen in Figure 5 and the consistency between "normal" (i.e., CaO-poor) melt inclusion compositions and experimental melts of peridotite (inserts Figure 7). Note that although the CaO concentration of the CaO-rich primitive melt inclusion population increases to values higher than those reached during experimental melting of peridotite, it remains well below the CaO contents expected for pure melts of amphibole-bearing olivine clinopyroxenites. Natural crustal pyroxenite cumulates such as the representative Duke Island amphibole-bearing olivine clinopyroxenites display a large range of CaO contents (from 13 to 24 wt%) [*Schiano et al.*, 2000]. Furthermore, CaO concentrations of pyroxenitic partial melts increase with increasing degrees of melting [*Médard et al.*, 2006]. As a consequence, the produced pyroxenitic liquids may display CaO contents up to 27 wt%.

Therefore, in order to generate melts with CaO contents similar to those of the CaO-rich melt inclusions from Pan de Azucar and Pichincha, a small proportion of liquids produced by melting of clinopyroxenite is required (less than 20 wt%). The addition of such a restricted proportion of pyroxenite melts will not significantly modify the arc-type trace element patterns of the melt inclusions, which explains why CaO-rich melt inclusions and peridotite-derived CaO-poor melt inclusions display similar trace element patterns and boron isotope compositions. Alternatively, the fact that melt inclusions with different CaO contents have similar trace element patterns may indicate that pyroxenitic melts have trace element characteristics close to peridotitic melts.

6.3. Slab Contribution

6.3.1. Across-Arc Variations

[34] Both Pichincha and Pan de Azucar melt inclusions display typical arc lava trace element patterns (Figure 6), which are generally interpreted in terms of slab contribution to the mantle wedge through the involvement of an H_2O-rich fluid phase released from the slab. However, trace elements variations in magmas are also controlled by differentiation processes; that is, the extent of partial melting and crystallization. Therefore, the behavior of trace elements during petrogenesis of arc magmas is directly related to their fluid/solid (M, for mobility) [*Tatsumi et al.*, 1986] and solid/melt (D) bulk partition coefficients during dehydration and differentiation processes, respectively. One way to distinguish between the effects of slab contribution and those of magmatic processes is to use ratios of incompatible elements with comparable D but distinct M values. Figure 8 shows the variations of concentration ratios of very incompatible elements whereby the fluid-mobile element (B, K, and Ba) is the numerator and the fluid-immobile element is the denominator. Melt inclusions from the front arc volcano Pichincha display higher fluid-mobile over less fluid-mobile element ratios than melt inclusions from the rear arc volcano Pan de Azucar, that are closer to MORB values (Figure 8). For instance, B/Nb ratios range from 5.0 to 11.9 for the Pichincha melt inclusions while they remain <1 for the Pan de Azucar melt inclusions (Figure 8b). A discrepancy in fluid-mobile element concentrations in the same order of magnitude is also observed for the whole rocks from the two volcanoes (open rectangles in Figure 8) [*Bourdon et al.*, 2003; *Hoffer*, 2008]. Such features are consistent with the cross-arc geochemical variations, typified by a systematic relationship between incompatible trace elements and the distance to the trench, previously reported for the Ecuadorian Andes [*Barragán et al.*, 1998] as well as for other volcanic arcs (Izu [*Ishikawa and Nakamura*, 1994], Kamchatka [*Ishikawa et al.*, 2001], and Andes [*Rosner et al.*, 2003; *Leeman and Sisson*, 1996]). This geochemical zoning could arise from (1) changes in the upper crust or (2) changes in the slab signal.

[35] On the basis of the observation that the North Andean crust varies systematically across the margin with respect to thickness, it has been proposed that an increase in the extent of crustal assimilation could be the origin of the cross arc variation for K_2O and incompatible trace elements for the Andean Northern volcanic zone [e.g., *Hildreth and Moorbath*, 1988]. However, the small range in stable and radiogenic isotopic variations of Ecuadorian lavas restricts to less than 10% the maximum amount of crustal assimilation [*Bryant et al.*, 2006]. As discussed in the work of *Barragán et al.* [1998], such a small amount cannot explain the variations of B, K, and Ba over Nb (or La) ratios observed in the Ecuadorian arc lavas. As these ratios are in the same order of magnitude for the melt inclusions and the bulk lavas, crustal contamination alone cannot account for the variations between the melt inclusions from Pichincha and Pan de Azucar. More evidence is brought by the B and $\delta^{11}B$ across-arc variations (Figure 8). The continental crust is enriched in B and has a negative $\delta^{11}B$ values (43 ppm B and $\delta^{11}B$ of $-8.9‰$, average values for the Andean crust) [*Kasemann et al.*, 2000]. If the increase in K_2O toward the rear arc is due to an increase of the amount of crustal contamination, then Pan de Azucar melt inclusions should be enriched in B compared to Pichincha melt inclusions. Figure 8 shows that this is not the case. Moreover, $\delta^{11}B$ values for Pan de Azucar melt inclusions are lower (up to $-17.9‰$) than the continental crust values. This is also consistent with the early entrapment of these melt inclusions in magnesium-rich olivines. Therefore, in the following, we will ignore the continental crust as a source of B.

[36] Elements such as B, K, and Ba are mobile in most fluids and when normalized to Nb or La, they may be used to track the role of slab-derived fluids. In terms of fluid-mobile elements, melt inclusions from Pichincha have significantly higher fluid-mobile element over Nb or La ratios than melt

Table 4. B, Nb, and δ^{11}B Compositions of the Mantle Wedge and the Slab Reservoirs[a]

	δ^{11}B (‰)	B (ppm)	Nb (ppm)	Nb/B
MW	−4.0[b]	0.05[b]	0.36[c]	7.20
AOC	+6.0[d]	10[e]	4.80[f]	0.48
SED	−6.6[g]	60[h]	2.50[i]	0.03

[a] MW is the mantle wedge, AOC is the altered oceanic crust, and SED is the sedimentary cover.
[b] N-MORB value from *Chaussidon and Marty* [1995].
[c] *Hofmann* [1988].
[d] *Rosner et al.* [2003], for the Central Andean AOC.
[e] Average of AOC values from DSP/ODP Hole 504b, 200 km south of the Galapagos spreading center (0.69 to 19.3 ppm) [*Ishikawa and Nakamura*, 1992].
[f] *Bailey* [1996].
[g] *Ishikawa and Nakamura* [1993].
[h] Within the range of pelagic sediments from *Ishikawa and Nakamura* [1993] (0 to 160 ppm of B).
[i] Value of site ODP 204 (Columbian trench) compiled by *Plank and Langmuir* [1998].

inclusions from Pan de Azucar; i.e., their compositions change with the depth of release from the slab toward MORB values (hatched area on Figure 8). In addition, Pichincha melt inclusions are characterized by more positive δ^{11}B values, a result that also indicates a change in the nature or the amount of the slab-derived components. However, Pan de Azucar melt inclusions show much higher La/Yb ratios (11.5 to 21.2) than the Pichincha melt inclusions (2.5–5.3). They are also enriched in incompatible elements such as K and LREE. This suggests that the Pan de Azucar melt inclusions were produced by lower degrees of melting. We thus speculate that the cross arc relationships recorded by the compositions of the melt inclusions reflect a decreasing contribution of the slab-derived fluids (and almost certainly differences in the nature of the fluids), which in turn would decrease the extent of melting. This model is similar to that proposed by *Barragán et al.* [1998] to explain the across-arc variations of Ecuadorian bulk lavas.

6.3.2. Characterization of the Slab Contribution

[37] The sediments and altered oceanic crust, which are parts of the descending slab, are enriched in boron (from 0 to 160 ppm for sediments [*Ishikawa and Nakamura*, 1993] and from 9 to 69 ppm for the altered oceanic crust [*Spivack and Edmond*, 1987]) whereas the upper mantle is characterized by low boron concentrations (0.05 ppm [*Chaussidon and Marty*, 1995]). The contrasting boron isotope compositions of altered oceanic crust (δ^{11}B from +0.1 ± 0.4‰ to +9.2 ± 0.4‰ [*Spivack and Edmond*, 1987]) and sediments (δ^{11}B from −17.0 ± 0.3‰ to +4.8 ± 0.1‰ for non-carbonate lithologies [*Ishikawa and Nakamura*, 1993]) allow us to discriminate between the relative contributions of these two reservoirs in the source of arc lavas. The variable δ^{11}B can also trace slab transfer mechanisms because ^{11}B fractionates preferentially into aqueous fluids whereas no fractionation occurs during partial melting [e.g., *Palmer et al.*, 1992]. The release of B and other fluid-mobile elements from the subducting slab into the overlying mantle wedge occurs by (1) progressive dehydration of the downgoing slab which releases fluids less and less enriched in boron and an associate decrease in their δ^{11}B compositions [*Peacock and Hervig*, 1999] or (2) a dehydration more dictated by the breakdown of hydrous phases in certain P-T intervals [e.g., *Ota et al.*, 2008].

[38] In this section, we attempt to model B concentrations and B isotope variations in the melt inclusions to decipher the nature of the slab input recorded by their compositions. Two different inputs can be envisioned: (1) fluids released during slab dehydration and (2) silicate melts derived from partial melting of the slab. In both case, the model follows three consecutive steps: (1) early dehydration of parts of the descending slab, namely the altered oceanic crust and sediments; then (2) metasomatism of the mantle wedge by the slab inputs (dehydrated fluids of silicate melts) under the volcanic arcs; and finally (3) melting of this metasomatized mantle. For the first step, the release of B from the slab is assumed to be a linear function of temperature; therefore we only consider a progressive dehydration similarly to what was proposed for the Chile subduction zone [*Rosner et al.*, 2003]. Since there is, to our knowledge, no precise boron isotope data on clinopyroxenites, we simplify the model by considering only the main peridotitic lithology as the mantle wedge before metasomatism (MW: 0.05 ppm B; δ^{11}B of −4.0 ± 1.6 ‰ [*Chaussidon and Marty*, 1995]; Table 4). Model parameters are presented in Table 4, and model results in Tables 5 and 6.

6.3.2.1. A Slab-Derived Metasomatic Aqueous Fluid Phase

[39] The hypothesis of a source metasomatized by slab-derived fluids is tested through the dehydration of the two slab components: the sediments (SED; Table 4) and the altered oceanic crust (AOC, Table 4) represented by the altered basalts from the Carnegie Ridge. The δ^{11}B values for the sediments

Table 5. Summary of the Results of the Model Reproducing the Compositions of Pichincha and Pan de Azucar Melt Inclusion Compositions by Metasomatism of the Mantle Wedge by Dehydration Fluids[a]

			Modeled Pichincha MI		Modeled Pan de Azucar MI	
Step			AOC	SED	AOC	SED
1	% of B loss in the reservoir		74	76	86	97
	% of H_2O loss in the reservoir		2.0	2.1	2.9	5.2
	slab-derived fluids	δ^{11}B (‰)	+3.5	−9.6	−0.8	−24
		B (ppm)	173	960	93	120
		Nb (ppm)	0	0	0	0
		Nb/B	0	0	0	0
2	% of fluid added into the MW		1		0.1	
	metasomatized MW	δ^{11}B (‰)	from +3.3 to −9.6		from −1.9 to −18.1	
		B (ppm)	from 2 to 6		from 0.15 to 0.20	
		Nb (ppm)	0.36		0.36	
		Nb/B	from 0.05 to 0.2		from 2 to 2.5	
3	% of partial melting of the metasomatized MW		25		0.1	
	melting of the metasomatized MW	δ^{11}B (‰)	from +3.3 to −9.6		from −1.9 to −18.1	
		B (ppm)	from 7 to 21		from 3 to 4	
		Nb (ppm)	1.3		7.3	
		Nb/B	from 0.05 to 0.2		from 2 to 2.5	

[a] Reservoir compositions are detailed in Table 4. AOC is altered oceanic crust; SED is sedimentary cover; MW is mantle wedge; MI is melt inclusion. Step 1 is early dehydration of the slab reservoir; step 2 is metasomatism of the mantle wedge by slab-derived fluids; step 3 is melting of the metasomatized mantle wedge. We assume that Nb is a highly incompatible in aqueous fluids. We consider a B isotopic fractionation between fluid and solid of +7‰ at 800°C [*Williams et al.*, 2001], a B partition coefficient between fluid and solid of 0.015 [e.g. *You et al.*, 1996], and a B bulk partition coefficient of 0.04 between the residue and the melt (calculated using the partition coefficients between the different minerals and a basaltic melt [*Chaussidon and Libourel*, 1993; *Adam and Green*, 2006], starting from a spinel lherzolite composition (KLB-1 [*Takahashi*, 1986]). If we add 25% of an amphibole-bearing olivine clinopyroxenite (OCA2 [*Médard et al.*, 2006]) to this source, the value of the bulk partition coefficient does not change significantly. We used the same partition coefficient between solid and melt for Nb and B [*Ryan et al.*, 1996], implying that the Nb/B ratio is not fractionated during partial melting.

Table 6. Summary of the Results of the Model Reproducing the Compositions of Pichincha and Pan de Azucar Melt Inclusion Compositions by Metasomatism of the Mantle Wedge by Silicate Melts[a]

			Modeled Pichincha MI		Modeled Pan de Azucar MI	
Step			AOC	SED	AOC	SED
1	% of B loss in the reservoir		30	35	65	90
	% of H_2O loss in the reservoir		0.5	0.7	1.6	3.4
	slab-derived melts	δ^{11}B (‰)	+3.5	−9.6	−1.4	−22.5
		B (ppm)	38	212	19	33
		Nb (ppm)	26	14	26	14
		Nb/B	>0.1	0.06	1.4	0.4
2	% of melts added into the MW		The model does		0.5–1%	
	metasomatized MW	δ^{11}B (‰)	not reproduce		from −1.9 to −18.2	
		B (ppm)	Pichincha MI		from 0.21 to 0.24	
		Nb (ppm)	compositions (see		from 0.4 to 0.6	
		Nb/B	text for details)		from 2 to 2.6	
3	% of partial melting of the metasomatized MW				1	
	melting of the metasomatized MW	δ^{11}B (‰)			from −1.9 to −18.2	
		B (ppm)			from 4 to 5	
		Nb (ppm)			from 8 to 12	
		Nb/B			from 2 to 2.6	

[a] See caption of Table 5 for details. To model slab partial melting, we used a similar melt/solid partition coefficient to the one used for mantle melting (0.04 for both B and Nb, see caption of Table 5), and a degree of melting of the slab of 15% [*Rapp et al.*, 1999].

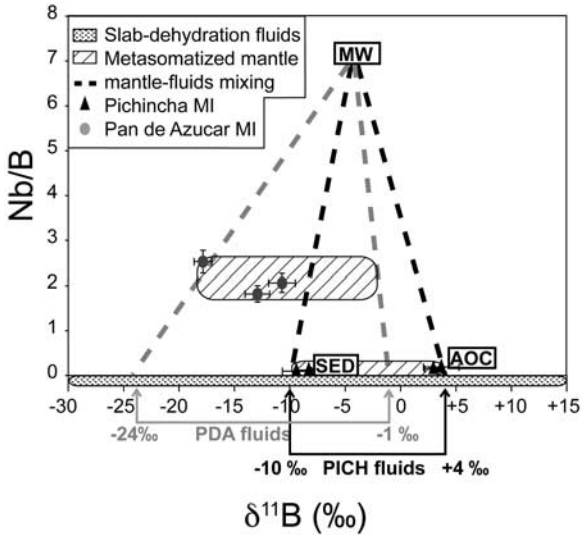

Figure 9. Modeling of the compositions in δ^{11}B and Nb/B of Pichincha and Pan de Azucar melt inclusions (MI) by metasomatism of the mantle wedge by slab-derived fluids. Because slab dehydration induces boron isotope fractionation (see text for details), all the fluids from the different stages of slab dehydration have different δ^{11}B values. However, they all have Nb/B values close to zero. Metasomatism of the mantle wedge can be expressed as mixing (dotted lines) between these dehydration fluids (dotted area) and the mantle reservoir (MW). The δ^{11}B values of fluids that modify the source of the melt inclusions (PICH fluids and PDA fluids) are determined by the linear fit between the mantle wedge compositions and the range of compositions of the respective melt inclusions. The parameters for the different components are from Table 4 and model parameters from Table 5. Errors bars are 1σ error of mean ($\sigma/\sqrt{n}$).

and AOC are taken from the literature and from geographical regions relevant to the present geological settings. The sedimentary cover of the Carnegie ridge consists of various pelagic sediments interbedded with chert horizons (ODP legs of site 1238 and 1239, off the Ecuadorian coast, on the Carnegie ridge) [*Mix et al.*, 2003]. The variable δ^{11}B values of modern marine sediments range from -6.6 ± 0.1 to $+4.8 \pm 0.1$‰ [*Ishikawa and Nakamura*, 1993]. The same authors also analyzed one Triassic chert, which has a δ^{11}B of -17.0 ± 0.1‰. To account for the presence of cherts in the Carnegie ridge sedimentary cover, we chose to use the most negative value of the pelagic sediments range (−6.6‰, Table 4). The Central Andean AOC is estimated to have a δ^{11}B value of +6.0‰ [*Rosner et al.*, 2003], which is similar to the average δ^{11}B values of the AOC from DSP/ODP Hole 504b, 200 km south of the Galapagos spreading center ($+2.2 \pm 0.1$ to $+10.6 \pm 0.2$‰) [*Ishikawa and Nakamura*, 1992].

[40] In the following discussion, starting from the composition of the Pichincha and Pan de Azucar melt inclusions, we assess the composition of the fluids that metasomatize the mantle wedge, and then we constrain the amount of dehydration of the slab required for the formation of these fluids. Plots of Nb/B versus δ^{11}B (Figure 9) and B versus δ^{11}B (Figure 10) are used to constrain the metasomatism of the mantle wedge and the dehydration of the slab, respectively.

[41] Nb and B have similar partition coefficients between solid and melt [*Kessel et al.*, 2005] during partial melting but one is a fluid-immobile element (Nb) and the other is fluid-mobile (B). They are commonly used to track slab-derived inputs in the source of arc magmas [e.g., *Ryan et al.*, 1996]. Boron isotopes do not fractionate at magmatic temperatures [*Palmer et al.*, 1992], therefore in a graph of Nb/B versus δ^{11}B, a melt will be superimposed on its source. In these conditions, the δ^{11}B and Nb/B values of the melt inclusions are similar to those of their sources (hatched area, Figure 9) and the Nb/B ratio of dehydration fluids is close to zero (dotted area in Figure 9) [e.g., *Ishikawa et al.*, 2001].

[42] In Figure 9, metasomatism of the mantle wedge can be expressed as mixing (dotted line, Figure 9) between these dehydration fluids and the mantle reservoir (MW, Figure 9). The difference in Nb/B between the source of the Pichincha melt inclusions and that of Pan de Azucar melt inclusions reflects different mixing proportions of fluids into the mantle: moving upward on a mixing line corresponds to a decrease in the fluid input into the mantle source. Therefore, the source of Pan de Azucar melt inclusions has been less metasomatized than that of Pichincha melt inclusions. This is in good agreement with the across-arc variations of trace elements ratios in the melt inclusions described previously.

[43] In the case of Pichincha, the fluids that modify the source of the melt inclusions are heterogeneous and have δ^{11}B varying between about −10‰ and +4‰ (dotted black lines, Figure 9). These values are the linear fit between the mantle wedge compositions and the range of compositions of the Pichincha melt inclusions on Figure 9. Therefore they correspond to the maximum and minimum values, respectively; that is, the range in the isotope composition of the metasomatizing fluids could be

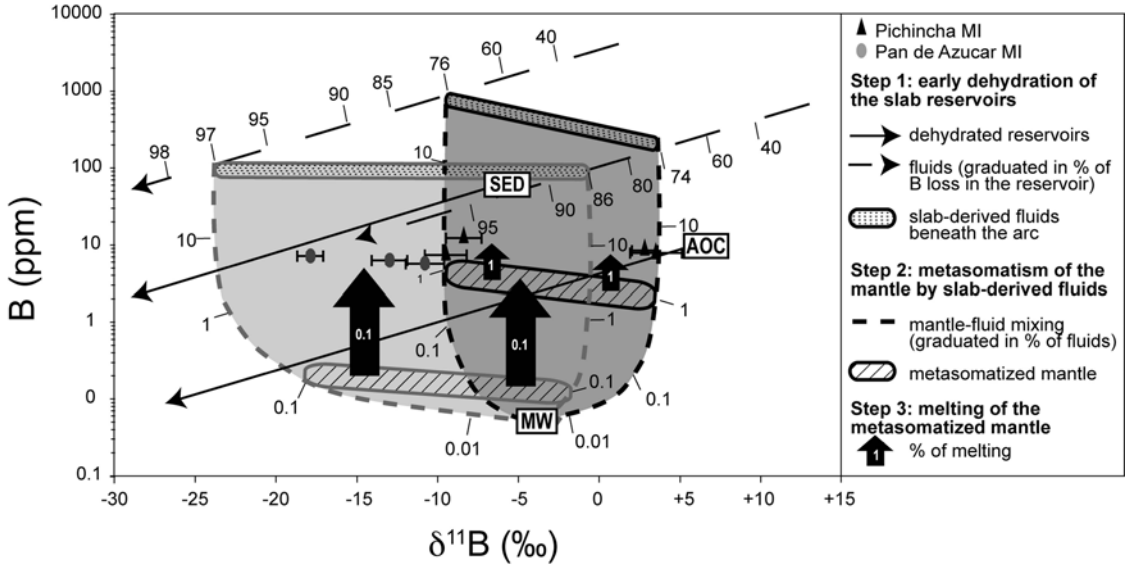

Figure 10. Modeling of the compositions in δ^{11}B and B of the Pichincha and Pan de Azucar melt inclusions (MI) by metasomatism of the mantle wedge by slab-derived fluids. The parameters for the different components are from Table 4 and model parameters from Table 5. Errors bars are 1σ error of mean ($\sigma/\sqrt{n}$).

larger. Similarly, the fluids that modify the source of Pan de Azucar melt inclusions are chemically heterogeneous and have δ^{11}B values between about −24‰ and −1‰ (dotted gray lines, Figure 9).

[44] During dehydration, both the B concentration and the δ^{11}B value of the slab residue decrease [e.g., *Bebout et al.*, 1993; *Gurenko et al.*, 2005]. At the same time, the fluids released are enriched in B compared to the residue. The first fluids released are extremely enriched in B due to the incompatible behavior of B. As the slab goes down, dehydration fluids become less enriched in B and less fractionated relative to the residue (due to the increase in temperature) [*Williams et al.*, 2001]. Therefore, the heterogeneous fluids that metasomatized the sources of the Pichincha and Pan de Azucar melt inclusions can be modeled by a mixing process between AOC-derived fluids (end-members with the highest δ^{11}B values) and SED-derived fluids (end-members with the lowest δ^{11}B values) at two different stages of dehydration (more dehydrated in the case of Pan de Azucar, where all the fluid end-members are shifted toward more negative δ^{11}B values).

[45] The variations of B and δ^{11}B in the melt inclusions were reproduced using a Rayleigh-type dehydration model of the slab components with instantaneous fluid compositions (Table 5 and Figure 10). Only the composition of the fluids released under the arc is relevant to this study, and not the first liquids released early into the accretionary prism. For that reason, a constant isotopic fractionation value, calculated at the temperature of the slab beneath the volcanic arc, is used in the model. In a young and hot subduction zone such as the Ecuador trench, the temperature under the arc reaches 800°C (thermal modeling from *Peacock* [2003], using the example of the Nankai warm subduction zone) and therefore the B isotope fractionation between fluids and solid is +7‰ [*Williams et al.*, 2001]. The Pichincha heterogeneous fluids can be reproduced by a mixing of fluids released after the AOC and SED lost 74 and 76% of B, respectively. This corresponds to a loss of 2.0 and 2.1‰ of initial H_2O, respectively (using a B partition coefficient between fluid and solid of 0.015 [e.g., *You et al.*, 1996], Figure 10, Table 5). These results are consistent with the fact that most of the boron is released before the volcanic arc, mainly in the accretionary prism [*Leeman and Sisson*, 1996]. The Pan de Azucar heterogeneous fluids can be reproduced by a mixing of fluids released after the AOC and SED lost 86 and 97% of B, respectively (which corresponds to a loss of 2.9 and 5.2% of initial H_2O, respectively; Figure 10, Table 5).

[46] Using these fluids compositions (Table 5), the calculated amount of fluids added in the mantle to reproduce Nb/B contents of the melt inclusions is 1% beneath Pichincha, whereas it decreases down to 0.1‰ beneath Pan de Azucar (Figure 10). This decrease in the slab input from the front arc to the

rear arc is in good agreement with the decrease in the B/Nb or Ba/Nb trace elements ratios described previously. Finally, a degree of melting of the metasomatized sources of the Pichincha and Pan de Azucar melt inclusions (with 2–6 and 0.15–0.20 ppm B, respectively) of 25% and 0.1% reproduces the B contents of the melt inclusions (Table 5). These degrees of melting are close to what has been proposed for the Ecuadorian lavas (15% for the front arc lavas, down to 2% for the rear arc lavas [*Barragán et al.*, 1998]). Moreover, the decrease in the degree of melting from the front arc to the rear arc is in good agreement with the decrease of the La/Yb ratio reported previously. However, the B and Nb concentrations of the modeled melts for Pan de Azucar (3–4 ppm and 7.3 ppm, respectively) are slightly lower than the B and Nb concentrations of Pan de Azucar melt inclusions (5–7 ppm and 11–18 ppm, respectively).

6.3.2.2. A Slab-Derived Metasomatic Silicate Melt Phase

[47] Previous studies on the Ecuadorian lavas have reported slab melts occurrences [e.g., *Monzier et al.*, 1997; *Bourdon et al.*, 2003; *Samaniego et al.*, 2005]. Therefore the metasomatic agent can also be derived from the melting of the subducting slab. The hypothesis of a source enriched by slab-derived melts was tested using a model of partial melting of the slab components (same components as the fluids metasomatism model, Table 4). First, the early dehydration of the slab was modeled in the same way as in the previous case for fluids (Rayleigh-type dehydration of slab reservoirs). Then the partially dehydrated residue melts beneath the arc. Melting occurs at a higher temperature than dehydration, so it does not produce a significant boron isotope fractionation [e.g., *Palmer et al.*, 1992]. Therefore the slab-derived melts will have the same δ^{11}B as the source reservoir. As Nb and B have similar solid-melt partition coefficients [*Kessel et al.*, 2005; *Ryan et al.*, 1996], the melts will also have the same Nb/B ratios as their source reservoir. In Figure 11, the B, Nb, and δ^{11}B compositions of the slab melts are calculated by a model of batch melting of both dehydrated SED and dehydrated AOC (Table 6). The dehydrated slab residue and their melts are superimposed during each step of dehydration (i.e., the black arrows representing the melting of the slab in Figure 11a become a point in Figure 11b, situated at the end of the dehydrated reservoirs arrows). During dehydration, δ^{11}B of the residue decreases, whereas Nb/B increases (Figures 11a and 11b).

[48] On the one hand, the model suggests that mixing between mantle (Nb/B of 7.2, Table 4) and AOC melts (Nb/B > 0.48, Figure 9, Table 6) cannot reproduce Pichincha melt inclusion compositions (Nb/B of 0.1–0.2). On the other hand, melting of the dehydrated SED only cannot generate the highest δ^{11}B measured in Pichincha melt inclusions (up to +3.2‰). Therefore, Pichincha melt inclusions cannot be derived from a mantle metasomatized by slab melts only. The possibility remains that both AOC-derived fluids and SED-derived melts took part in the formation of Pichincha melt inclusions. However, this model is more complex and was not considered here because the model of a source metasomatized by fluids satisfactorily explains the compositions of Pichincha melt inclusions.

[49] In the case of Pan de Azucar, the compositions of the melt inclusions (Nb/B of 1.8–2.5) can result from a mixing event between mantle melts and both dehydrated AOC-derived melts and dehydrated SED-derived melts. Melts with δ^{11}B of −1.4‰ and −22.5‰ can be generated from the melting of the dehydrated AOC and SED components, after 65 and 90% of B loss, respectively (i.e., 1.6% and 3.4% of H_2O loss, respectively, Figure 11, Table 6). After the addition of 0.5–1% of these melts to the mantle wedge, and after 1% of melting of this metasomatized source, the melts produced contain 4–5 ppm of B and 8–12 ppm of Nb (Table 6). The results of the latter model are more consistent with the compositions of Pan de Azucar melt inclusions than those of a model of metasomatism by dehydration fluids. This is in good agreement with the conclusions of *Hoffer et al.* [2008], where the lavas from the Ecuadorian rear-arc are interpreted as a result of the partial melting of a mantle metasomatized by slab melts.

7. Conclusion

[50] As major element compositions of the Pichincha and the Pan de Azucar melt inclusions do not fall on a continuous extension of the trends defined by the host lava suites, they cannot be related to these suites through low-pressure fractionation paths. They define a distinct population of primitive, nepheline-normative magmas characterized by high CaO concentrations, which are not

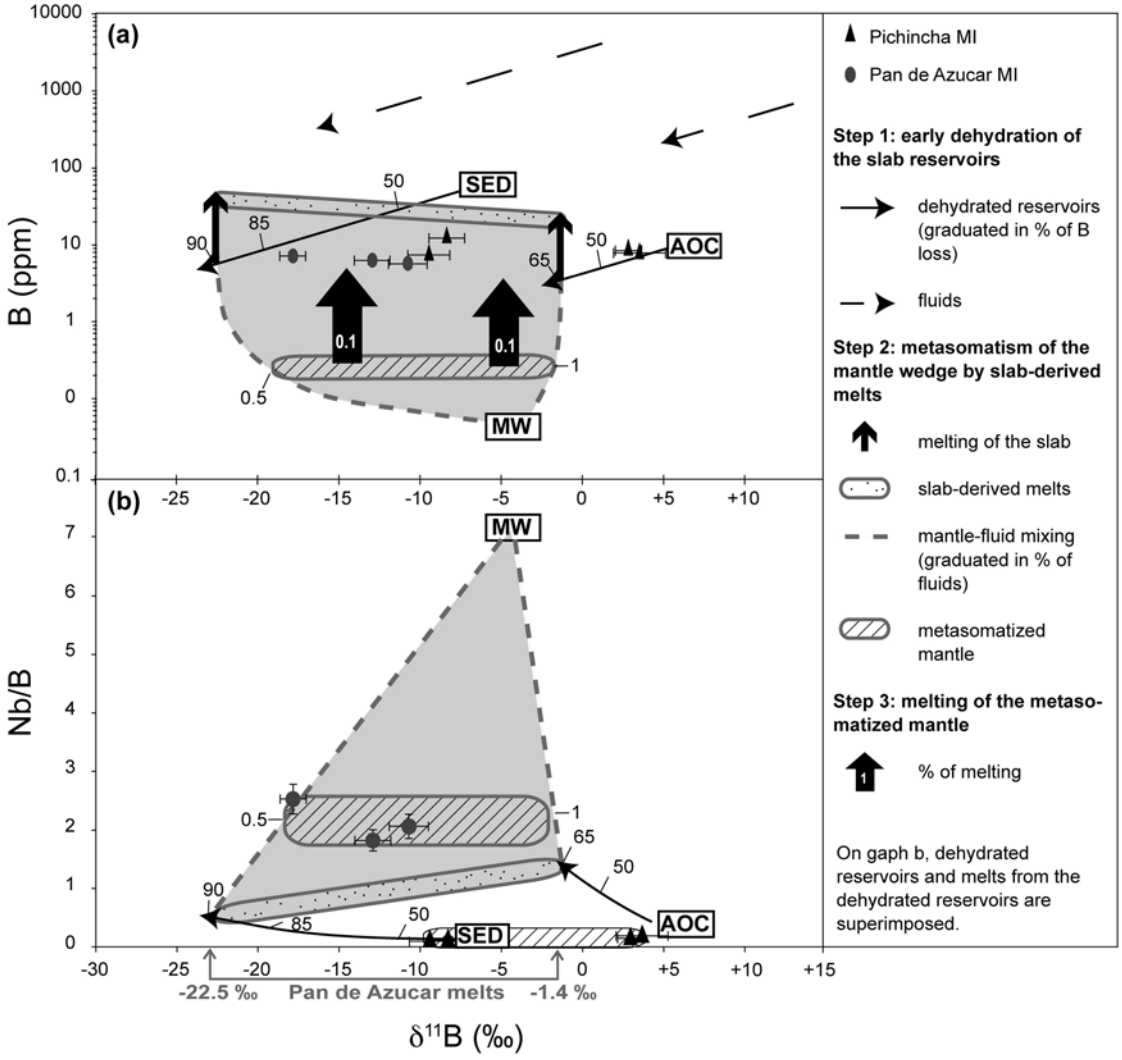

Figure 11. Modeling of the compositions in $\delta^{11}B$, (a) B, and (b) Nb/B of Pan de Azucar melt inclusions (MI) by metasomatism of the mantle wedge by slab-derived melts. The parameters for the different components are from Table 4 and model parameters from Table 6. Errors bars are 1σ error of mean ($\sigma/\sqrt{n}$).

Table A1. Detail of Electron Microprobe Replicate Measurements on VG-A99 Basaltic Glass[a]

	Over One Session (This Study)		Over 1 Year[b]		USGS[c]	
VG-A99	n = 10 Mean	Standard Deviation	n = 10 Mean	Standard Deviation	n = 10 Mean	Standard Deviation
Na_2O	2.67	0.10	2.73	0.11	2.72	0.16
MgO	4.99	0.08	5.02	0.09	5.04	0.1
K_2O	0.85	0.04	0.86	0.03	0.82	0.03
CaO	9.12	0.05	9.13	0.09	9.04	0.11
TiO_2	4.18	0.05	4.17	0.07	3.95	0.09
FeO	13.08	0.22	13.24	0.31	13.15	0.16
MnO	0.23	0.07	0.20	0.06	0.19	0.02
SiO_2	50.80	0.19	51.11	0.54	51.06	0.46
Al_2O_3	12.51	0.12	12.66	0.15	12.44	0.13
P_2O_5	0.48	0.06	0.46	0.05	0.43	0.03
Total	98.90		99.30		98.84	

[a] Average compositions and standard deviation in wt%.
[b] J. L. Devidal (personal communication, 2008); 1 year of routine analysis of VG-A99 on the Cameca SX 100 electron microprobe at LMV, Clermont-Ferrand.
[c] From *Thorner et al.* [2002].

expressed as bulk lavas. Their origin is attributed to a mixing between partial melts of amphibole-bearing olivine clinopyroxenite lithologies (similar to those found in lower crustal or shallow upper mantle cumulates in arc environments) and of peridotitic lithologies. These results give further support to the assertion that such magmas occur in arcs around the world and contribute early to the host lava history [*Schiano et al.*, 2000].

[51] Trace elements and boron isotope compositions of the melt inclusions indicate that the across-arc geochemical changes previously reported for the Ecuadorian Andes are likely to result from the change of the slab input with increasing slab depth, and from the variation of the sediment-derived component. The slab component that metasomatizes the source of the Pichincha melt inclusions can be attributed to a heterogeneous fluid that is derived from both sediment and altered oceanic crust sources. The component that metasomatizes the source of the Pan de Azucar melt inclusions can be either a heterogeneous aqueous fluid or a heterogeneous silicate melt, both derived from different degrees of dehydration of altered oceanic crust and sediments. However, B and Nb concentrations in Pan de Azucar melt inclusions are better reproduced with the model of slab melt metasomatism.

Appendix A

[52] Appendix A contains Table A1 showing a detail of electron microprobe replicate measurements on VG-A99 basaltic glass.

Acknowledgments

[53] This paper is dedicated to the memory of Jean-Philippe Eissen, who initiated this project, and provided the Pichincha samples. The authors are grateful to G. Hoffer for providing the Pan de Azucar samples. This study has benefited from constructive discussions with K. Koga, J.-L. Le Pennec, E. Médard, P. Samaniego, E. Bourdon, S. Lambart, and A.-S. Bouvier. Special thanks go to the following persons: J.-L. Devidal for technical assistance with the electron microprobe and N. Shimizu, D. Mangin, M. Champenois, and C. Rollion-Bard for their precious help with the ion microprobe. This study was supported by an ANR "Jeune Chercheur" grant (2006, CNRS, France) to E. Rose-Koga. The authors would like to thank V. Salters, G. Bebout R. Tanaka, A. Gurenko, and an anonymous reviewer for their constructive reviews and comments.

References

Adam, J., and T. Green (2006), Trace element partitioning between mica- and amphibole-bearing garnet lherzolite and hydrous basanitic melt: 1. Experimental results and the investigation of controls on partitioning behaviour, *Contrib. Mineral. Petrol.*, *152*, 1–17, doi:10.1007/s00410-006-0085-4.

Bailey, J. C. (1996), Role of subducted sediments in the genesis of Kurile-Kamchatka island arc basalts; Sr isotopic and elemental evidence, *Geochem. J.*, *30*, 289–321.

Baker, M. B., and E. M. Stolper (1994), Determining the composition of high-pressure mantle melts using diamond aggregates, *Geochim. Cosmochim. Acta*, *58*, 2811–2827, doi:10.1016/0016-7037(94)90116-3.

Baker, M. B., M. M. Hirschmann, M. S. Ghiorso, and E. M. Stolper (1995), Compositions of near-solidus peridotite melts from experiments and thermodynamic calculations, *Nature*, *375*, 308–311, doi:10.1038/375308a0.

Baronnet, A. (1984), Growth kinetics of the silicates - A review of basic concepts, *Fortschr. Mineral.*, *62*, 187–232.

Barragán, R., D. Geist, M. L. Hall, P. Larson, and M. Kurz (1998), Subduction controls on the compositions of lavas from the Ecuadorian Andes, *Earth Planet. Sci. Lett.*, *154*, 153–166, doi:10.1016/S0012-821X(97)00141-6.

Beattie, P. (1994), Systematics and energetics of trace-element partitioning between olivine and silicate melts: Implications for the nature of mineral/melt partitioning, *Chem. Geol.*, *117*, 57–71, doi:10.1016/0009-2541(94)90121-X.

Bebout, G. E., J. G. Ryan, and W. P. Leeman (1993), B-Be systematics in subduction-related metamorphic rocks: Characterization of the subducted component, *Geochim. Cosmochim. Acta*, *57*, 2227–2237, doi:10.1016/0016-7037(93)90565-E.

Bourdon, E., J.-P. Eissen, M.-A. Gutscher, M. Monzier, M. L. Hall, and J. Cotten (2003), Magmatic response to early aseismic ridge subduction: The Ecuadorian margin case (South America), *Earth Planet. Sci. Lett.*, *205*, 123–138, doi:10.1016/S0012-821X(02)01024-5.

Bryant, J. A., G. M. Yogodzinski, M. L. Hall, J. L. Lewicki, and D. G. Bailey (2006), Geochemical constraints on the origin of volcanic rocks from the Andean Northern Volcanic Zone, Ecuador, *J. Petrol.*, *47*, 1147–1175, doi:10.1093/petrology/egl006.

Chaussidon, M., and G. Libourel (1993), Boron partitioning in the upper mantle: An experimental and ion probe study, *Geochim. Cosmochim. Acta*, *57*, 5053–5062, doi:10.1016/0016-7037(93)90607-X.

Chaussidon, M., and B. Marty (1995), Primitive boron isotope composition of the mantle, *Science*, *269*, 383–386, doi:10.1126/science.269.5222.383.

Dalton, J., and D. C. Presnall (1998), The continuum of primary carbonatitic-kimberlitic melt compositions in equilibrium with lherzolites: Data from the system CMAS-CO at 6 GPa, *J. Petrol.*, *39*, 1953–1964, doi:10.1093/petrology/39.11.1953.

Danyushevsky, L. V., F. N. Della-Pasqua, and S. Sokolov (2000), Re-equilibration of melt inclusions trapped by magnesian olivine phenocrysts from subduction-related magmas: Petrological implications, *Contrib. Mineral. Petrol.*, *138*, 68–83, doi:10.1007/PL00007664.

Danyushevsky, L. V., R. A. J. Leslie, A. J. Crawford, and P. Durance (2004), Melt inclusions in primitive olivine phenocrysts: The role of localized reaction processes in the origin of anomalous compositions, *J. Petrol.*, *45*, 2531–2553, doi:10.1093/petrology/egh080.

Fahey, A. J., E. K. Zinner, G. Crozaz, and A. S. Kornacki (1987), Microdistributions of Mg isotopes and REE abundances in a Type A calcium-aluminum-rich inclusion from Efremovka, *Geochim. Cosmochim. Acta*, *51*, 3215–3229, doi:10.1016/0016-7037(87)90130-X.

Falloon, T. J., L. V. Danyushevsky, and D. H. Green (2001), Peridotite melting at 1 GPa: Reversal experiments on partial melts compositions produced by peridotite-basalt sandwich experiments, *J. Petrol.*, *42*, 2363–2390, doi:10.1093/petrology/42.12.2363.

Faure, F., and P. Schiano (2005), Experimental investigation of equilibration conditions during forsterite growth and melt inclusion formation, *Earth Planet. Sci. Lett.*, *236*, 882–898, doi:10.1016/j.epsl.2005.04.050.

Fornari, M., M. Monzier, P. Samaniego, C. Robin, B. Beate, E. Bourdon, J.-P. Eissen, and G. Féraud (2004), Ar-Ar dating of active quaternary Pichincha volcano, Quito, Ecuador, paper presented at 1st General Assembly, Eur. Geosci. Union, Nice, France.

Gaetani, G. A., and T. L. Grove (1998), The influence of water on melting of mantle peridotite, *Contrib. Mineral. Petrol.*, *131*, 323–346, doi:10.1007/s004100050396.

Garrison, J. M., and J. P. Davidson (2003), Dubious case for slab melting in the Northern volcanic zone of the Andes, *Geology*, *31*, 565–568, doi:10.1130/0091-7613(2003)031<0565:DCFSMI>2.0.CO;2.

Gill, J. G. (1981), *Orogenic Andesites and Plate Tectonics*, 390 pp., Springer, New York.

Green, D. H., and A. E. Ringwood (1967), The genesis of basaltic magma, *Contrib. Mineral. Petrol.*, *15*, 103–190, doi:10.1007/BF00372052.

Guillier, B., J.-L. Chatelain, É. Jaillard, H. Yepes, G. Poupinet, and J.-F. Fels (2001), Seismological evidence on the geometry of the orogenic system in central-northern Ecuador (South America), *Geophys. Res. Lett.*, *28*, 3749–3752, doi:10.1029/2001GL013257.

Gurenko, A. A., and M. Chaussidon (1995), Enriched and depleted primitive melts included in olivine from Icelandic tholeiites: Origin by continuous melting of a single mantle column, *Geochim. Cosmochim. Acta*, *59*, 2905–2917, doi:10.1016/0016-7037(95)00184-0.

Gurenko, A. A., R. B. Trumbull, R. Thomas, and J. M. Lindsay (2005), A melt inclusion record of volatiles, trace elements and Li-B isotope variations in a single magma system from the Plat Pays Volcanic Complex, Dominica, Lesser Antilles, *J. Petrol.*, *46*, 2495–2526, doi:10.1093/petrology/egi063.

Gutscher, M.-A., J.-L. Olivet, D. Aslanian, J.-P. Eissen, and R. C. Maury (1999), The "lost Inca Plateau": Cause of flat subduction beneath Peru?, *Earth Planet. Sci. Lett.*, *171*, 335–341, doi:10.1016/S0012-821X(99)00153-3.

Hervig, R. L., G. M. Moore, L. B. Williams, S. M. Peacock, J. R. Holloway, and K. Roggensack (2002), Isotopic and elemental partitioning of boron between hydrous fluid and silicate melt, *Am. Mineral.*, *87*, 769–774.

Hidalgo, S., M. Monzier, H. Martin, G. Chazot, J.-P. Eissen, and J. Cotten (2007), Adakitic magmas in the Ecuadorian Volcanic Front: Petrogenesis of the Iliniza Volcanic Complex (Ecuador), *J. Volcanol. Geotherm. Res.*, *159*, 366–392, doi:10.1016/j.jvolgeores.2006.07.007.

Hildreth, W., and S. Moorbath (1988), Crustal contributions to arc magmatism in the Andes of Central Chile, *Contrib. Mineral. Petrol.*, *98*, 455–489, doi:10.1007/BF00372365.

Hirose, K. (1997), Partial melt compositions of carbonated peridotite at 3 GPa and role of CO_2 in alkali-basalt magma generation, *Geophys. Res. Lett.*, *24*, 2837–2840, doi:10.1029/97GL02956.

Hirose, K., and T. Kawamoto (1995), Hydrous partial melting of lherzolite at 1 GPa: The effect of H_2O on the genesis of basaltic magmas, *Earth Planet. Sci. Lett.*, *133*, 463–473, doi:10.1016/0012-821X(95)00096-U.

Hirose, K., and I. Kushiro (1993), Partial melting of dry peridotites at high pressures: Determination of compositions of melts segregated from peridotite using aggregates of diamond, *Earth Planet. Sci. Lett.*, *114*, 477–489, doi:10.1016/0012-821X(93)90077-M.

Hirschmann, M. M., and M. Pertermann (2000), Application of MELTS to pyroxenite partial melting in basalt source regions, *J. Conf. Abstr.*, *5*, 519.

Hirschmann, M. M., M. B. Baker, and E. M. Stolper (1998), The effect of alkalis on the silica content of mantle-derived melts, *Geochim. Cosmochim. Acta*, *62*, 883–902, doi:10.1016/S0016-7037(98)00028-3.

Hirschmann, M. M., T. Kogiso, M. B. Baker, and E. M. Stolper (2003), Alkalic magmas generated by partial melting of garnet pyroxenite, *Geology*, *31*, 481–484, doi:10.1130/0091-7613(2003)031<0481:AMGBPM>2.0.CO;2.

Hoffer, G. (2008), Fusion partielle d'un manteau métasomatisé par un liquide adakitique: Approches géochimique et expérimentale de la genèse et de l'évolution des magmas de l'arrière-arc équatorien, Ph.D. thesis, 320 pp, Blaise Pascal Univ., Clermont-Ferrand, France.

Hoffer, G., J.-P. Eissen, B. Beate, E. Bourdon, M. Fornari, and J. Cotten (2008), Geochemical and petrological constraints on rear-arc magma genesis processes in Ecuador: The Puyo cones and Mera lavas volcanic formations, *J. Volcanol. Geotherm. Res.*, *176*, 107–118, doi:10.1016/j.jvolgeores.2008.05.023.

Hofmann, A. W. (1988), Chemical differentiation of the Earth: The relationship between mantle, continental crust and oceanic crust, *Earth Planet. Sci. Lett.*, *90*, 297–314, doi:10.1016/0012-821X(88)90132-X.

Ishikawa, T., and E. Nakamura (1992), Boron isotope geochemistry of the oceanic crust from DSDP/ODP Hole 504B, *Geochim. Cosmochim. Acta*, *56*, 1633–1639, doi:10.1016/0016-7037(92)90230-G.

Ishikawa, T., and E. Nakamura (1993), Boron isotope systematics of marine sediments, *Earth Planet. Sci. Lett.*, *117*, 567–580, doi:10.1016/0012-821X(93)90103-G.

Ishikawa, T., and E. Nakamura (1994), Origin of the slab component in arc lavas from across-arc variation of B and Pb isotopes, *Nature*, *370*, 205–208, doi:10.1038/370205a0.

Ishikawa, T., F. Tera, and T. Nakazawa (2001), Boron isotope and trace element systematics of the three volcanic zones in the Kamchatka arc, *Geochim. Cosmochim. Acta*, *65*, 4523–4537, doi:10.1016/S0016-7037(01)00765-7.

Ito, K., and G. C. Kennedy (1974), The composition of liquids formed by partial melting of eclogites at high temperatures and pressures, *J. Geol.*, *82*, 383–392.

Jarosewich, E., A. S. Parkes, and L. B. Wiggins (1979), Microprobe analyses of four natural glasses and one mineral: An interlaboratory study of precision and accuracy, *Smithson. Contrib. Earth Sci.*, *22*, 53–67.

Jochum, K. P., et al. (2006), MPI-DING reference glasses for in situ microanalysis: New reference values for element concentrations and isotope ratios, *Geochem. Geophys. Geosyst.*, *7*, Q02008, doi:10.1029/2005GC001060.

Jugo, P. J., R. W. Luth, and J. P. Richards (2005), Experimental data on the speciation of sulfur as a function of oxygen fugacity in basaltic melts, *Geochim. Cosmochim. Acta*, *69*, 497–503, doi:10.1016/j.gca.2004.07.011.

Kasemann, S., J. Erzinger, and G. Franz (2000), Boron recycling in the continental crust of the central Andes from the Paleozoic to Mezozoic, NW Argentina, *Contrib. Mineral. Petrol.*, *140*, 328–343, doi:10.1007/s004100000189.

Keshav, S., G. H. Gudfinnsson, G. Sen, and Y. Fei (2004), High-pressure melting experiments on garnet clinopyroxenite and the alkalic to tholeiitic transition in ocean-island basalts, *Earth Planet. Sci. Lett.*, *223*, 365–379, doi:10.1016/j.epsl.2004.04.029.

Kessel, R., M. W. Schmidt, P. Ulmer, and T. Pettke (2005), Trace element signature of subduction-zone fluids, melts and supercritical liquids at 120–180 km depth, *Nature*, *437*, 724–727, doi:10.1038/nature03971.

Kilinc, A., I. S. E. Carmichael, M. L. Rivers, and R. O. Sack (1983), The Ferric-Ferrous ratio of natural silicate liquids equilibrated in air, *Contrib. Mineral. Petrol.*, *83*, 136–140, doi:10.1007/BF00373086.

Kogiso, T., and M. Hirschmann (2001), Experimental study of clinopyroxenite partial melting and the origin of ultra-calcic melt inclusions, *Contrib. Mineral. Petrol.*, *142*, 347–360.

Kogiso, T., and M. M. Hirschmann (2006), Partial melting experiments of bimineralic eclogite and the role of recycled mafic oceanic crust in the genesis of ocean island basalts, *Earth Planet. Sci. Lett.*, *249*, 188–199, doi:10.1016/j.epsl.2006.07.016.

Kogiso, T., K. Hirose, and E. Takahashi (1998), Melting experiments on homogeneous mixtures of peridotite and basalt: Application to the genesis of ocean island basalts, *Earth Planet. Sci. Lett.*, *162*, 45–61, doi:10.1016/S0012-821X(98)00156-3.

Kogiso, T., M. M. Hirschmann, and D. J. Frost (2003), High-pressure partial melting of garnet pyroxenite: Possible mafic lithologies in the source of ocean island basalts, *Earth Planet. Sci. Lett.*, *216*, 603–617, doi:10.1016/S0012-821X(03)00538-7.

Kogiso, T., M. M. Hirschmann, and M. Pertermann (2004), High-pressure partial melting of mafic lithologies in the mantle, *J. Petrol.*, *45*, 2407–2422, doi:10.1093/petrology/egh057.

Kushiro, I. (1996), Partial melting of a fertile mantle peridotite at high pressures: An experimental study using aggregates of diamond, in *Earth Processes: Reading the Isotopic Code*, *Geophys. Monogr. Ser.*, vol. 95, edited by A. Basu and S. Hart, pp. 109–022, AGU, Washington, D. C.

Langmuir, C. H., A. Bézos, S. Escrig, and S. Parman (2006), Chemical systematics and hydrous melting of the mantle in back-arc basins, in *Back-Arc Spreading Systems: Geological, Biological, Chemical, and Physical Interactions*, *Geophys. Monogr. Ser.*, vol. 166, edited by D. M. Christie et al., pp. 87–146, AGU, Washington, D. C.

Laubier, M., P. Schiano, R. Doucelance, L. Ottolini, and D. Laporte (2007), Olivine-hosted melt inclusions and melting processes beneath the FAMOUS zone (Mid-Atlantic Ridge), *Chem. Geol.*, *240*, 129–150, doi:10.1016/j.chemgeo.2007.02.002.

Leeman, W. P., and V. B. Sisson (1996), Geochemistry of boron and its implications for crustal and mantle processes, in *Boron Mineralogy, Petrology and Geochemistry*, *Rev. in Mineral.*, vol. 33, edited by E. S. Grew and L. M. Anovitz, pp. 646–708, Mineral. Soc. of Am., Washington, D. C.

Médard, E., M. W. Schmidt, P. Schiano, and L. Ottolini (2006), Melting of amphibole-bearing wehrlites; an experiment study on the origin of ultra-calcic nepheline-normative melts, *J. Petrol.*, *47*, 481–504, doi:10.1093/petrology/egi083.

Mix, A. C., et al. (2003), Site 1238 and 1239, *Proc. Ocean Drill. Program, Init. Rep.*, *202*, 93 pp.

Monzier, M., C. Robin, M. L. Hall, J. Cotten, P. Mothes, J.-P. Eissen, and P. Samaniego (1997), Les adakites d'Équateur: Modèle préliminaire, *C. R. Acad. Sci., Ser. II*, *324*, 545–552.

Monzier, M., C. Robin, M. L. Hall, J. Cotten, and P. Samaniego (1999), Geochemistry and tectonics at the southern termination of the Northern volcanic zone (Riobamba volcanoes, Ecuador); preliminary results, paper presented at 4th International Symposium on Andean Geodynamics, Inst. de Rech. pour le Dev., Göttingen, Germany.

Monzier, M., et al. (2002), Evolution of the Pichincha volcanic complex (Ecuador), paper presented at 5th International Symposium on Andean Geodynamics, Inst. de Rech. pour le Dev., Toulouse, France.

Morris, J. D., W. P. Leeman, and F. Tera (1990), The subducted component in island arc lavas: Constraints from Be isotopes and B-Be systematics, *Nature*, *344*, 31–36, doi:10.1038/344031a0.

O'Hara, M. J. (1972), Data reduction and projection schemes for complex compositions, *Prog. Exp. Petrol.*, *3*, 103–126.

Ota, T., K. Kobayashi, T. Katsura, and E. Nakamura (2008), Tourmaline breakdown in a pelitic system: Implications for boron cycling through subduction zones, *Contrib. Mineral. Petrol.*, *155*, 19–23, doi:10.1007/s00410-007-0228-2.

Palmer, M. R., and J. F. Slack (1989), Boron isotopic compositions of tourmaline from massive sulfide deposits and tourmalinites, *Contrib. Mineral. Petrol.*, *103*, 434–451, doi:10.1007/BF01041751.

Palmer, M. R., and G. H. Swihart (1996), Boron isotope geochemistry; an overview, in *Boron: Mineralogy, Petrology and Geochemistry*, edited by E. S. Grew and L. M. Anovitz, pp. 709–744, Mineral. Soc. of Am., Washington, D. C.

Palmer, M. R., D. London, V. Morgan, and H. A. Babb (1992), Experimental determination of fractionation of $^{11}B/^{10}B$ between tourmaline and aqueous vapor: A temperature- and pressure-dependent isotopic system, *Chem. Geol.*, *101*, 123–129.

Peacock, S. M. (2003), Thermal structure and metamorphic evolution of subducting slabs, in *Inside the Subduction Factory*, *Geophys. Monogr. Ser.*, vol. 138, edited by J. Eiler, pp. 7–22, AGU, Washington, D. C.

Peacock, S. M., and R. L. Hervig (1999), Boron isotopic composition of subduction-zone metamorphic rocks, *Chem. Geol.*, *160*, 281–290, doi:10.1016/S0009-2541(99)00103-5.

Pertermann, M., and M. M. Hirschmann (2003), Anhydrous partial melting experiments on MORB-like eclogite; phase relations, phase compositions and mineral-melt partitioning of major elements at 2–3 GPa, *J. Petrol.*, *44*, 2173–2201, doi:10.1093/petrology/egg074.

Pickering-Witter, J., and A. D. Johnston (2000), The effects of variable bulk composition on the melting systematics of fertile peridotitic assemblages, *Contrib. Mineral. Petrol.*, *140*, 190–211, doi:10.1007/s004100000183.

Plank, T., and C. H. Langmuir (1998), The chemical composition of subducting sediment and its consequences for the crust and mantle, *Chem. Geol.*, *145*, 325–394, doi:10.1016/S0009-2541(97)00150-2.

Rapp, R. P., N. Shimizu, M. D. Norman, and G. S. Applegate (1999), Reaction between slab-derived melts and peridotite in the mantle wedge: Experimental constraints at 3.8 GPa, *Chem. Geol.*, *160*, 335–356, doi:10.1016/S0009-2541(99)00106-0.

Reynaud, C., É. Jaillard, H. Lapierre, M. Mamberti, and G. H. Mascle (1999), Oceanic plateau and island arcs of southwestern Ecuador: Their place in the geodynamic evolution of northwestern South America, *Tectonophysics*, *307*, 235–254, doi:10.1016/S0040-1951(99)00099-2.

Robinson, J. A. C., B. J. Wood, and J. D. Blundy (1998), The beginning of melting of fertile and depleted peridotite at 1.5 GPa, *Earth Planet. Sci. Lett.*, *155*, 97–111, doi:10.1016/S0012-821X(97)00162-3.

Roedder, E. (1984), *Fluid Inclusions*, *Rev. Mineral.*, vol. 12, 644 pp., Mineral. Soc. of Am., Washington, D. C.

Rosner, M., J. Erzinger, G. Franz, and R. B. Trumbull (2003), Slab-derived boron isotope signatures in arc volcanic rocks from the Central Andes and evidence for boron isotope fractionation during progressive slab dehydration, *Geochem. Geophys. Geosyst.*, *4*(8), 9005, doi:10.1029/2002GC000438.

Rosner, M., M. Wiedenbeck, and T. Ludwig (2008), Composition-induced variations in SIMS instrumental mass fractionation during boron isotope ratio measurements of silicate glasses, *Geostand. Geoanal. Res.*, *32*, 27–38, doi:10.1111/j.1751-908X.2008.00875.x.

Ryan, J. G., W. P. Leeman, J. D. Morris, and C. H. Langmuir (1996), The boron systematics of intraplate lavas: Implications for crust and mantle evolution, *Geochim. Cosmochim. Acta*, *60*, 415–422, doi:10.1016/0016-7037(95)00402-5.

Saal, A. E., S. R. Hart, N. Shimizu, E. H. Hauri, and G. D. Layne (1998), Pb isotopic variability in melt inclusions from oceanic island basalts, Polynesia, *Science*, *282*, 1481–1484, doi:10.1126/science.282.5393.1481.

Samaniego, P., H. Martin, M. Monzier, C. Robin, M. Fornari, J.-P. Eissen, and J. Cotten (2005), Temporal evolution of magmatism in the northern volcanic zone of the Andes: The geology and petrology of Cayambe Volcanic Complex (Ecuador), *J. Petrol.*, *46*, 2225–2252, doi:10.1093/petrology/egi053.

Schiano, P. (2003), Primitive mantle magmas recorded as silicate melt inclusions in igneous minerals, *Earth Sci. Rev.*, *63*, 121–144, doi:10.1016/S0012-8252(03)00034-5.

Schiano, P., and B. Bourdon (1999), On the preservation of mantle information in ultramafic nodules: Glass inclusions within minerals versus interstitial glasses, *Earth Planet. Sci. Lett.*, *169*, 173–188, doi:10.1016/S0012-821X(99)00074-6.

Schiano, P., J. M. Eiler, I. D. Hutcheon, and E. M. Stolper (2000), Primitive CaO-rich, silica-undersaturated melts in island arcs: Evidence for the involvement of clinopyroxene-rich lithologies in the petrogenesis of arc magmas, *Geochem. Geophys. Geosyst.*, *1*(5), 1018, doi:10.1029/1999GC000032.

Schiano, P., R. Clocchiatti, L. Ottolini, and A. Sbrana (2004), The relationship between potassic, calc-alcaline and Na-alcaline magmatism in South Italy volcanoes: A melt inclusion approach, *Earth Planet. Sci. Lett.*, *220*, 121–137, doi:10.1016/S0012-821X(04)00048-2.

Schwab, B. E., and A. D. Johnston (2001), Melting systematics of modally variable, compositionally intermediate peridotites and the effects of mineral fertility, *J. Petrol.*, *42*, 1789–1811, doi:10.1093/petrology/42.10.1789.

Sobolev, A. V. (1996), Melt inclusions in minerals as a source of principle petrological information, *Petrology*, *4*, 209–220.

Sobolev, A. V., and N. Shimizu (1993), Ultra-depleted primary melt included in an olivine from the Mid-Atlantic Ridge, *Nature*, *363*, 151–154, doi:10.1038/363151a0.

Spivack, A. J., and J. M. Edmond (1987), Boron isotope exchange between seawater and the oceanic crust, *Geochim. Cosmochim. Acta*, *51*, 1033–1043, doi:10.1016/0016-7037(87)90198-0.

Takahashi, E. (1986), Melting of a dry peridotite KLB-1 up to 14 GPa: Implications on the origin of peridotitic upper mantle, *J. Geophys. Res.*, *91*, 9367–9382, doi:10.1029/JB091iB09p09367.

Takahashi, E., K. Nakajima, and T. L. Wright (1998), Origin of the Columbia River basalts: Melting model of a heterogeneous plume head, *Earth Planet. Sci. Lett.*, *162*, 63–80, doi:10.1016/S0012-821X(98)00157-5.

Tatsumi, Y., and S. Eggins (1995), *Subduction Zone Magmatism*, *Frontiers in Earth Sci.*, 211 pp., Blackwell Sci., Cambridge, U. K.

Tatsumi, Y., D. L. Hamilton, and R. W. Nesbitt (1986), Chemical characteristics of fluid phase released from a subducted lithosphere and origin of arc magmas: Evidence from high-pressure experiments and natural rocks, *J. Volcanol. Geotherm. Res.*, *29*, 293–309, doi:10.1016/0377-0273(86)90049-1.

Thorner, K. R., D. R. Sherrod, D. F. Siems, C. Christina Heliker, G. P. Meeker, R. L. Oscarson, and J. P. Kauahikaua (2002), Whole-rock and glass major-element geochemistry of Kilauea Volcano, Hawaii, near-vent eruptive products:

September 1994 through September 2001, *U.S. Geol. Surv. Open File Rep.*, *02-17*, 9 pp.

Toplis, M. J. (2005), The thermodynamics of iron and magnesium partitioning between olivine and liquid: Criteria for assessing and predicting equilibrium in natural and experimental systems*Contrib. Mineral. Petrol.*, *149*, 22–39, doi:10.1007/s00410-004-0629-4.

Trenkamp, R., J. N. Kellogg, J. T. Freymueller, and H. P. Mora (2002), Wide plate margin deformation, southern Central America and northwestern South America, CASA GPS observations, *J. S. Am. Earth Sci.*, *15*, 157–171, doi:10.1016/S0895-9811(02)00018-4.

Van Thournout, F., J. Hertogen, and L. Quevedo (1992), Allochtonous terranes in northwestern Ecuador, *Tectonophysics*, *205*, 205–221, doi:10.1016/0040-1951(92)90427-8.

Walter, M. J. (1998), Melting of garnet peridotite and the origin of komatiite and depleted lithosphere, *J. Petrol.*, *39*, 29–60, doi:10.1093/petrology/39.1.29.

Wasylenki, L. E. (1998), Partial melting of depleted peridotite in the Earth's upper mantle and implications for generation of mid-ocean ridge basalts, Ph.D. thesis, Calif. Inst. of Technol., Pasadena.

Wasylenki, L. E., M. B. Baker, A. J. R. Kent, and E. M. Stolper (2003), Near-solidus melting of the shallow upper mantle: Partial melting experiments on depleted peridotite, *J. Petrol.*, *44*, 1163–1191, doi:10.1093/petrology/44.7.1163.

Weaver, S. J., and C. H. Langmuir (1990), Calculation of phase equilibrium in mineral-melt systems*Comput. Geosci.*, *16*, 1–19, doi:10.1016/0098-3004(90)90074-4.

Williams, L. B., R. L. Hervig, J. R. Holloway, and I. Hutcheon (2001), Boron isotope geochemistry during diagenesis. Part I. Experimental determination of fractionation during illitization of smectite, *Geochim. Cosmochim. Acta*, *65*, 1769–1782, doi:10.1016/S0016-7037(01)00557-9.

You, C. F., A. J. Spivack, J. M. Gieskes, J. B. Martin, and M. L. Davisson (1996), Boron contents and isotopic compositions in pore waters; a new approach to determine temperature induced artifacts; geochemical implications, *Mar. Geol.*, *129*, 351–361, doi:10.1016/0025-3227(96)83353-6.